




Rapid growth of a carbonate island over the last millennium

MARJORIE CANTINE* , EMILY ORZECZOWSKI†, NATHAN STEIN‡·§ ,
TYLER LINCOLN¶, BRIANNA HIBNER¶, THEODORE PRESENT‡ ,
MICHAEL THORPE**, JUSTIN STRAUSS††,
ANELIZE MANUELA BAHNIUK RUMBELSPERGER‡‡, ANDREW H. KNOLL§§,
JOHN GROTZINGER‡, MAYA GOMES¶¶ and ELIZABETH TROWER¶¶

*Department of Earth and Space Sciences, 1707 NE Grant Lane, University of Washington, Seattle, WA 98195, USA (E-mail: cantine@uw.edu)

†National Climate Adaptation Center, United States Geological Survey, 12201 Sunrise Valley Drive, Reston, Virginia 20192, USA

‡Division of Geological and Planetary Sciences, Caltech, 1200 E California Blvd, Pasadena, California 91125, USA

§Epirus Inc., P.O. Box 3927, Redondo Beach, California 90277, USA

¶Department of Geological Sciences, University of Colorado Boulder, UCB 399, Boulder, Colorado 80309-0399, USA

**CRESST II, NASA GSFC, University of Maryland, 8800 Greenbelt Rd, Greenbelt, Maryland 20771, USA

††Department of Earth Sciences, Dartmouth College, HB 6105, Hanover, New Hampshire 03755, USA

‡‡Universidade Federal do Paraná – Geologia, Av. Cel. Francisco H. dos Santos, 210 - Jardim das Américas - Curitiba (PR), Curitiba, Paraná, Brazil

§§Department of Organismic and Evolutionary Biology, Harvard University, 26 Oxford St, Cambridge, Massachusetts 02138, USA

¶¶Department of Earth and Planetary Sciences, The Johns Hopkins University, 3400 North Charles Street, Baltimore, Maryland 21218, USA

Associate Editor – Rick Sarg

ABSTRACT

Low-lying islands in tropical regions are vulnerable to near-term sea-level rise and hurricane-induced flooding, with substantial human impact. These risks motivate researchers to elucidate the processes and timescales involved in the formation, growth and stabilization of coastlines through the study of Holocene shoreline dynamics. Little Ambergris Cay (Turks and Caicos Islands) is a low-lying carbonate island that provides a case study in the nucleation and growth of such islands. This study investigates the sedimentology and radiocarbon chronology of the island's lithified sediments to develop a model for its history. The island's lithified rim encloses a tidal swamp populated by microbial mats and mangroves. Preliminary radiocarbon data supported a long-standing inference that the island is Holocene in age. This study integrates petrographic, sedimentological and new radiocarbon data to quantify the age of the island and develop a model for its evolution. Results indicate that the ages of most lithified sediments on the island are <1000 cal yr BP, and the generation and lithification of carbonate sediment in this system supports coastline growth of at least 5 cm/year. The lithification of anthropogenic detritus was documented, consistent with other evidence that in recent centuries the lithified rim has grown by rates up to tens of centimetres per year. A unit of mid-Holocene age was identified and correlated with a similar unit of early transgressive aeolianite described from San Salvador, The Bahamas. It is proposed that this antecedent feature played an important role in the nucleation and formation of the modern

island. Results extend an established Bahamian stratigraphic framework to the south-western extreme of the Lucayan archipelago, and highlight the dynamism of carbonate shorelines, which should inform forward-looking mitigation strategies to increase coastal resiliency to sea-level rise. These results inform interpretation of the palaeoenvironmental record of carbonate environments, underscoring their geologically rapid pace of lithification.

Keywords Carbonate sedimentology, Holocene, radiocarbon, Turks & Caicos Islands.

INTRODUCTION

Global mean sea level is predicted to rise by as much as a metre or more by the year 2100 (Horton *et al.*, 2020). This projected sea-level rise may enhance damage caused by hurricanes (Strauss *et al.*, 2021), increase the frequency and magnitude of coastal flooding (Kirezci *et al.*, 2020) and cause land loss (Nicholls, 2011). The populations, infrastructure and ecosystems of low-lying, hurricane-prone regions are especially vulnerable to these changes. Such near-term trends – and their potential human impact – call for the study of Holocene shorelines and the processes that contribute to their nucleation, growth and stabilization, which include early lithification, the impact of storms, sediment supply and sediment delivery by wind, waves and longshore currents. Motivated by these concerns, this study investigates a Caribbean island, Little Ambergris Cay (Turks and Caicos Islands), and leverages the carbonate sedimentology and radiocarbon chronology of its lithified rim to develop a model for island nucleation and growth over the Holocene.

Little Ambergris Cay is an excellent location to study the dynamics of a natural carbonate Holocene shoreline. The cay is uninhabited, and so anthropogenic modification of the environment is minimal. Preliminary radiocarbon data (Orzechowski *et al.*, 2016; Stein *et al.*, 2023) support the long-standing inference that Little Ambergris Cay is Holocene in age (Dravis & Wanless, 2017). Over the Holocene Epoch, sea level in the Caribbean region has risen by tens of metres (Khan *et al.*, 2017). Meltwater input from the Laurentide ice sheet drove rapid relative sea-level rise during the early Holocene at rates as high as 10.9 ± 0.6 m/ka, followed by slower relative sea-level rise, driven by glacial isostatic adjustment, at rates $<2.4 \pm 0.4$ m/ka after about 7 ka (Milne *et al.*, 2005; Milne &

Peros, 2013; Khan *et al.*, 2017). For most areas in the Caribbean, current sea level is thought to be at or near its Holocene maximum (Khan *et al.*, 2017).

Many other carbonate islands across the Lucayan archipelago have grown by Holocene sediment accumulation and progradation on Pleistocene antecedents (Peter & Gould, 1984; Strasser & Davaud, 1986; Kindler & Hearty, 1996; Maloof & Grotzinger, 2012; Dravis & Wanless, 2017; Kerans *et al.*, 2019). Little Ambergris Cay is unusual in that it appears to lack a lithified Pleistocene antecedent, recording instead entirely Holocene island nucleation, growth and lithification. For this reason, Little Ambergris Cay provides a case study of the geological and sedimentological processes that form carbonate islands and sustain coastlines over geologically short timescales. The history of the island may highlight mechanisms capable of enhancing the resiliency of coastlines and slowing or reversing land loss at human timescales as both sea level and the marine carbon cycle change in the coming century.

GEOLOGICAL BACKGROUND

The Caicos Platform, located in the eastern Caribbean (Fig. 1A) is a wind-dominated carbonate platform (Wanless *et al.*, 1989; Dravis & Wanless, 2008, 2017). Strong, persistent trade winds blow from the east year-round, driving westward sediment transport (Trower *et al.*, 2018). Little Ambergris Cay, a wetland nature reserve, sits approximately 2 km leeward of Big Ambergris Cay, its larger, privately-owned sister island (Fig. 1B).

Big Ambergris Cay is a 5 km long island running roughly north–south near the south-east edge of the platform. It has been an important study site for herpetologists (Gerber *et al.*, 2020;

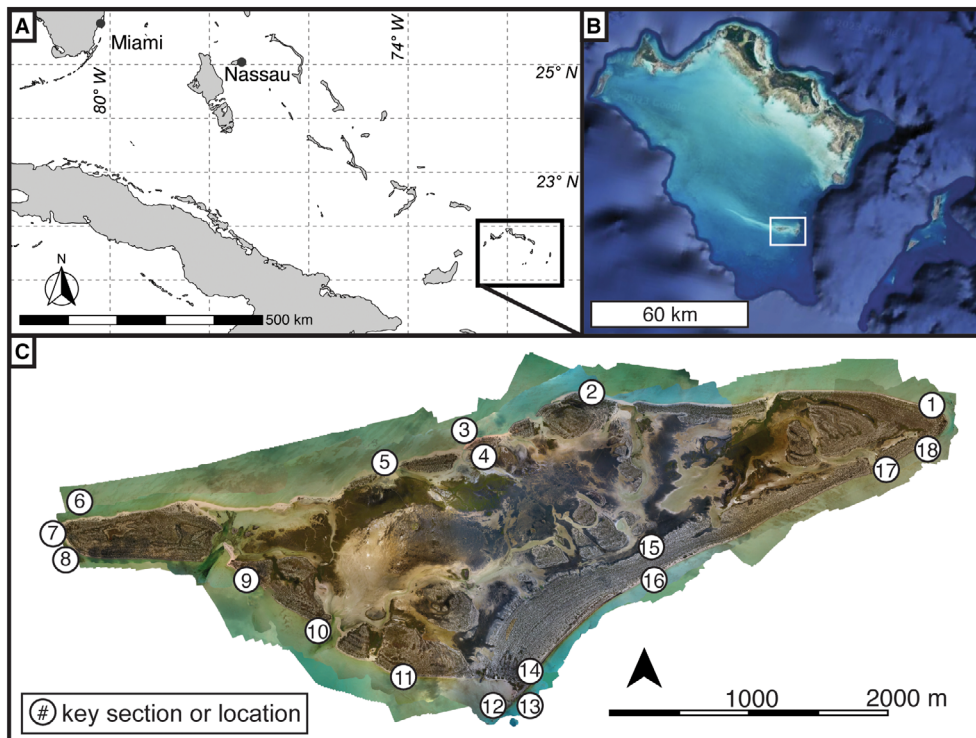


Fig. 1. (A) Regional map with the Turks and Caicos platforms in black rectangle. (B) Satellite image of the Turks and Caicos platforms. Big and Little Ambergris Cays marked with white rectangle. Imagery from Google Earth©. (C) Orthomosaic imagery of Little Ambergris Cay in summer 2017. Locations and sections referenced in the main text of this study are indicated with circled numbers. See Table 1 for coordinates of these sections and [Supporting Information](#) for details of other sections.

Reynolds *et al.*, 2020) and botanists (Hardman *et al.*, 2012) researching species endemic to the Turks and Caicos Islands. Topography on Big Ambergris Cay reaches up to 25 m or more above sea level (Dravis & Wanless, 2017); its bedrock geology has not been described in detail but is presumed to be Pleistocene in age (Dravis & Wanless, 2017). Little Ambergris Cay (Fig. 1C) is about 6 km long and 1.6 km wide at its maximum. It is oriented east–west. The island is a wetland nature reserve protected by the Department of Environmental and Coastal Resources of the Turks and Caicos Islands and the Turks and Caicos National Trust. A 20 km long, linear ooid shoal continues westward from the west tip of the island (Lloyd *et al.*, 1987; Dravis & Wanless, 2008, 2017; Rankey *et al.*, 2008; Trower *et al.*, 2018). Little Ambergris Cay has lower relief than Big Ambergris Cay; the highest point on the island is only 4.5 m above sea level, with an average elevation of 1.1 m (Stein *et al.*, 2023).

The perimeter of Little Ambergris Cay consists of a lithified rim locally breached by tidal channels, with a strandplain along the island's south-eastern shore (Fig. 1C) (Orzechowski *et al.*, 2016). The island's interior is lower in elevation than its rim, and it is inundated by tides daily (Stein *et al.*, 2023). This interior lagoon hosts mangrove thickets and thick microbial mats. Previous investigations of Little Ambergris Cay have focused on its ooid shoal (Rankey *et al.*, 2008; Duguid *et al.*, 2010; Dravis & Wanless, 2017; Trower *et al.*, 2018), its mangrove and microbial ecosystems (Trembath-Reichert *et al.*, 2016; Raven *et al.*, 2019; Gomes *et al.*, 2020; Ward *et al.*, 2020; Lingappa *et al.*, 2022; Stein *et al.*, 2023), the taphonomy of its microbial mats (Gomes *et al.*, 2020; Present *et al.*, 2021) and the island's response to Hurricane Irma (Jamison-Todd *et al.*, 2020; Lingappa *et al.*, 2022). This study builds on previous work (Orzechowski *et al.*, 2016; Stein *et al.*, 2023) that confirmed the island's inferred Holocene age (Dravis &

Table 1. Names and coordinates of stratigraphic sections on Little Ambergris Cay documented in the main text of this study. Details of additional stratigraphic sections available in Appendix S1.

| Number in Map | Section name | Latitude | Longitude |
|---------------|--------------|--------------|--------------|
| 1 | EN1-J18 | N 21.304912° | W 71.66529° |
| 2 | CL | N 21.3057° | W 71.68843° |
| 3 | 15-C2 | N 21.30118° | W 71.70218° |
| 4 | 14-C2 | N 21.30083° | W 71.70178° |
| 5 | WC2 | N 21.29989° | W 71.70575° |
| 6 | BT | N 21.297367° | W 71.7245° |
| 7 | 12-LLAC | N 21.296132° | W 71.725402° |
| 8 | 8/8 LI-1 | N 21.29548° | W 71.72497° |
| 9 | WBB2 | N 21.29311° | W 71.71223° |
| 10 | WBBRO | N 21.289831° | W 71.70797° |
| 11 | 8/9 BB-5 | N 21.28658° | W 71.70222° |
| 12 | 8/6 FA-3 | N 21.284149° | W 71.695115° |
| 13 | 8/6 FA-2 | N 21.284537° | W 71.694621° |
| 14 | 8/6 FA-4 | N 21.285907° | W 71.693341° |
| 15 | WOS | N 21.295313° | W 71.684439° |
| 16 | 05-SS | N 21.29341° | W 71.68465° |
| 17 | 12A-SS | N 21.30093° | W 71.66882° |
| 18 | 10-SS | N 21.30283° | W 71.6657° |

Wanless, 2017), adding sedimentological and stratigraphic context along with new radiocarbon dates to provide a more complete depositional history of the island. Multiple lines of evidence support nucleation and growth of the island over the last millennium.

METHODS

Field campaigns took place during the summers of 2016, 2017, 2018, 2019 and 2022, as well as February 2023. During these campaigns, the lithified sediments on the island were described and photographed. Stratigraphic sections along the perimeter of the island were measured, and samples were taken for radiocarbon analysis and petrographic characterization.

Stratigraphy and facies analysis

Stratigraphic sections of the lithified rim and outcrops within the island interior were measured. The geographical coordinates of each section were recorded, and the base of every coastal section was within the modern intertidal zone. A Jacobs staff or ruler was used to measure bed thickness, and the sedimentological characteristics of the rock units were noted. Over the course of the field seasons, dozens of stratigraphic columns were measured. In the main text of this study, findings are summarized by presenting 18 sections (Table 1), representative of spatial and facies trends across the island on both the north (Fig. 2) and south (Fig. 3) coasts. Additional stratigraphic sections are included in Table S1 and Appendix S1.

During the autumn following the 2017 summer field season, Hurricane Irma passed directly over the island, exposing fresh outcrop in the island interior in erosional scour pits (Stein *et al.*, 2017; Jamison-Todd *et al.*, 2020). Hurricane Fiona also passed near the island in autumn 2022. Sections initially measured during the 2016 to 2018 field seasons were revisited during 2022 and 2023, given the possibility of fresh exposures following hurricane erosion. These field seasons also added multiple new stratigraphic sections, especially along the south-eastern shore and in the island interior.

Radiocarbon measurements

Sampling for radiocarbon focused on shell material lithified within rock in stratigraphic context (Table 2). Where shell material was not available, ooid grainstone was sampled instead. For samples from section 10, WBBRO, the facies of the samples are well-documented, but their precise stratigraphic locations are not recorded. For sample FA-4A from section 14, 8/6 FA-4, the stratigraphic position of the sample within the section is not known. These uncertainties are reflected in the corresponding stratigraphic columns (Fig. 3).

Individual shells were subsampled upon return to home laboratories and then sent for further analysis either at the University of California Irvine Keck Carbon Cycle AMS facility (UCIAMS; Beverly *et al.*, 2010) or at the National Ocean Sciences AMS (NOSAMS; Pearson *et al.*, 1997). At both facilities, samples were leached with dilute hydrochloric acid prior to hydrolysis with 85% phosphoric acid before

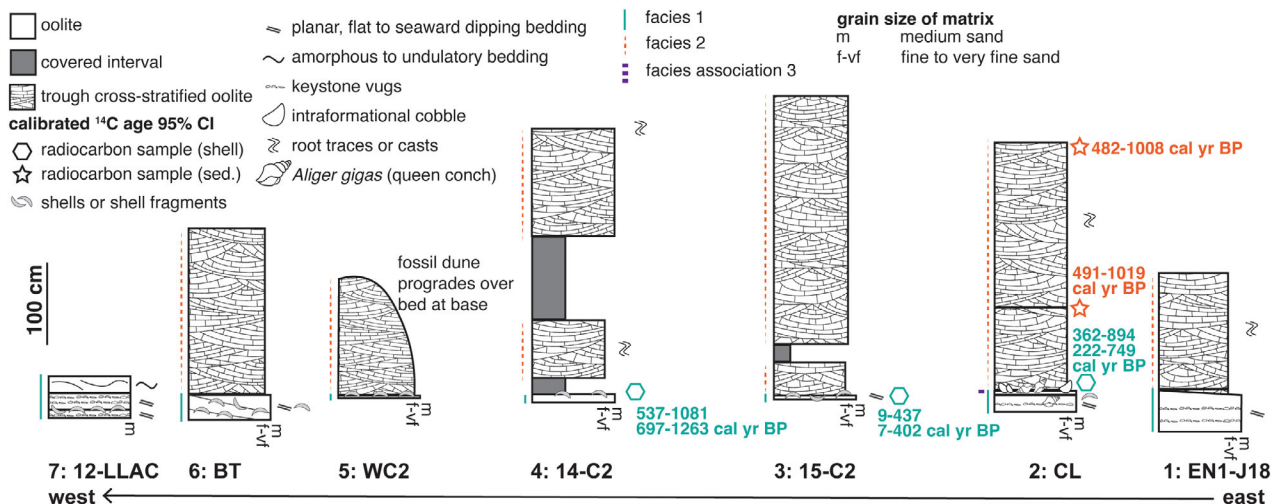


Fig. 2. Stratigraphic sections and calibrated radiocarbon dates from the north side of Little Ambergris Cay. Both foreshore and aeolian facies are present on the north side of the island, but the exposure of foreshore units is more limited than sections from the south side of the island. See Table 1 for coordinates of these sections and Table 2 for details of radiocarbon data.

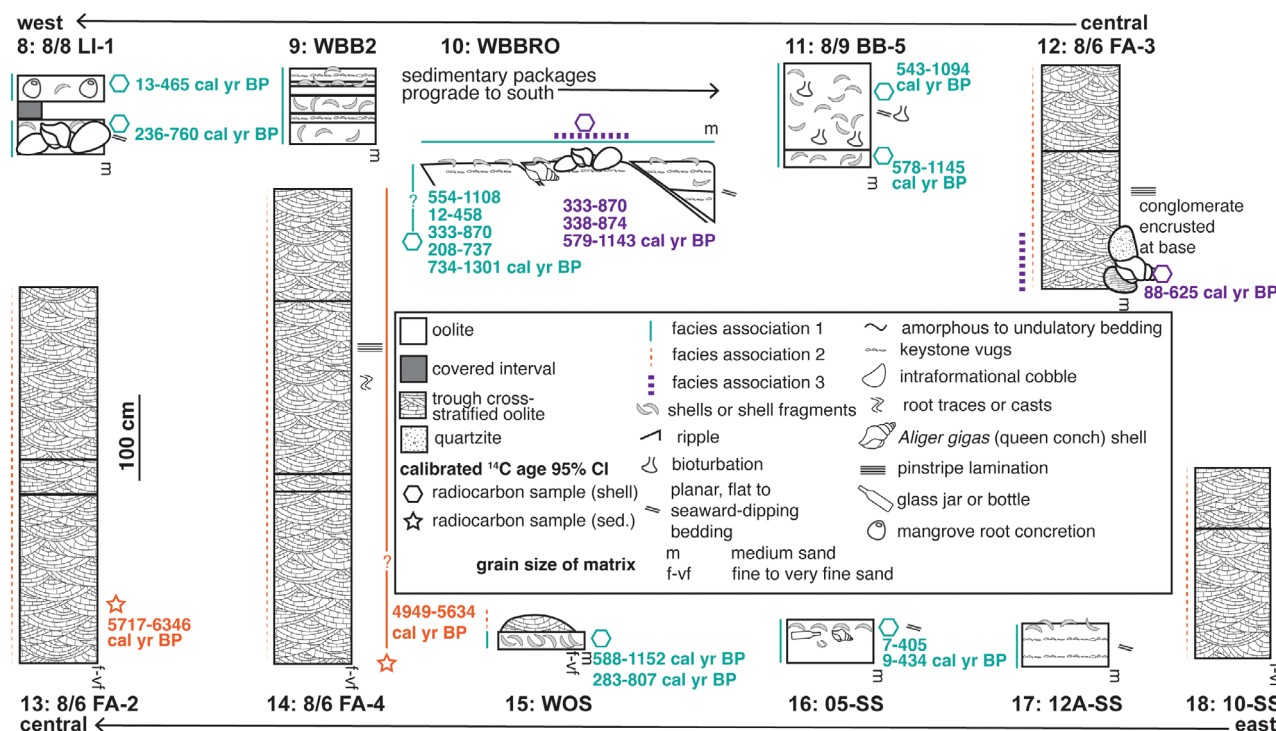


Fig. 3. Stratigraphic sections and calibrated radiocarbon dates from the south side of Little Ambergris Cay. Foreshore facies are better exposed on the south side of the island than the north. See Table 1 for coordinates of these sections and Table 2 for details of radiocarbon data.

Table 2. Radiocarbon results and calibrated ages for samples from Little Ambergis Cay.

| AMS ID | AMS | Sample name | Section number and name | Height or depth in section/core (cm) | Latitude | Longitude | Sample type | Facies | Fraction modern | ¹⁴ C age (yr BP) | Uncert | Credible interval, calibrated using Marine20 and $\Delta R = -230 \pm 131$ years (yr BP; 95% CI) | |
|--|----------|-------------------------|--|---|--------------|--------------|-------------|----------|-----------------|-----------------------------|--------|--|----------|
| SAMPLES FROM THE NORTHERN SHORE | | | | | | | | | | | | | |
| 184876 | NOSAMS | CL-01 shell 1 | 2: CL | 25 | N 21.3057° | W 71.68843° | Shell | Facies 1 | 0.8852 | 0.0018 | 980 | 15 | 362–894 |
| 184877 | NOSAMS | CL-01 shell 2 | | 25 | | | Shell | Facies 1 | 0.9005 | 0.0016 | 840 | 15 | 222–749 |
| 184879 | NOSAMS | CL-02 | | 125 | | | Sediment | Facies 2 | 0.8718 | 0.0017 | 1100 | 15 | 491–1019 |
| 184880 | NOSAMS | CL-03 | | 325 | | | Sediment | Facies 2 | 0.8736 | 0.0016 | 1090 | 15 | 482–1008 |
| 182392 | NOSAMS | LAC22-M-20a | 3: 15-C2 | 0 | N 21.30118° | W 71.70218° | Shell | Facies 1 | 0.9445 | 0.0018 | 460 | 15 | 9–437 |
| 182393 | NOSAMS | LAC22-M-20b | | 0 | | | Shell | Facies 1 | 0.9517 | 0.0020 | 400 | 15 | 7–402 |
| 182390 | NOSAMS | LAC22-M-18a | 4: 14-C2 | 10 | N 21.30083° | W 71.70178° | Shell | Facies 1 | 0.8656 | 0.0015 | 1160 | 15 | 537–1081 |
| 182391 | NOSAMS | LAC22-M-18b | | 10 | | | Shell | Facies 1 | 0.8443 | 0.0017 | 1360 | 15 | 697–1263 |
| SAMPLES FROM THE SOUTHERN SHORE | | | | | | | | | | | | | |
| 218532 | UCI Keck | 8/8 LI-1A shell | 8: 8/8 LI-1 | 40 | N 21.29548° | W 71.72497° | Shell | Facies 1 | 0.8998 | 0.0017 | 850 | 15 | 236–780 |
| 218533 | UCI Keck | 8/8 LI-1B shell | | 90 | | | Shell | Facies 1 | 0.9388 | 0.0020 | 505 | 20 | 13–465 |
| 218537 | UCI Keck | 8/5 BB-1B shell | No section, collected from beach facies | Not collected within section | N 21.29379° | W 71.71358° | Shell | Facies 1 | 0.9391 | 0.0018 | 505 | 15 | 13–464 |
| 218538 | UCI Keck | 8/5 BB-1A shell | | | | | Shell | Facies 1 | 0.9417 | 0.0018 | 480 | 20 | 11–451 |
| 181086 | UCI Keck | BBwf-1 | 10: WBBRO | Not recorded | N 21.288831° | W 71.70797° | Shell | Facies 1 | 0.8629 | 0.0016 | 1185 | 15 | 554–1108 |
| 181087 | UCI Keck | BBwf-2 | | | | | Shell | Facies 1 | 0.9760 | 0.0015 | 495 | 15 | 12–458 |
| 181088 | UCI Keck | BBwf-3 | | | | | Shell | Facies 1 | 0.8886 | 0.0014 | 950 | 15 | 333–870 |
| 181092 | UCI Keck | Bsil-1 | | | | | Shell | Facies 1 | 0.9020 | 0.0015 | 830 | 15 | 208–737 |
| 181095 | UCI Keck | Bsil-2 | | | | | Shell | Facies 1 | 0.8397 | 0.0013 | 1405 | 15 | 734–1301 |
| 181090 | UCI Keck | BBID-1 | | | | | Shell | Facies 3 | 0.8886 | 0.0013 | 950 | 15 | 333–870 |
| 181091 | UCI Keck | BBID-2 | | | | | Shell | Facies 3 | 0.8877 | 0.0014 | 955 | 15 | 338–874 |
| 181093 | UCI Keck | BBID-3 | | | | | Shell | Facies 3 | 0.8591 | 0.0013 | 1220 | 15 | 579–1143 |
| 218536 | UCI Keck | 8/9 BB01-A shell | Collected from section 8/9 BB-1 (not a key section; see Supplement for strat column) | 30 | N 21.288118° | W 71.706024° | Shell | Facies 1 | 0.8636 | 0.0016 | 1180 | 20 | 550–1105 |
| 218534 | UCI Keck | 8/9 BB-5B shell 1 | 11: 8/9 BB-5 | 20 | N 21.28658° | W 71.70222° | Shell | Facies 1 | 0.8593 | 0.0018 | 1220 | 20 | 578–1145 |
| 218535 | UCI Keck | 8/9 BB-5B shell 2 | | 120 | | | Shell | Facies 1 | 0.8643 | 0.0019 | 1170 | 20 | 543–1094 |
| 218541 | UCI Keck | FA-3A (breccia) shell 1 | 12: FA-3 | Collected from conglomerate accreted on outcrop | N 21.284149° | W 71.695115° | Shell | Facies 1 | 0.9153 | 0.0018 | 710 | 20 | 88–625 |

Table 2. (continued)

| AMS ID | AMS | Sample name | Section number and name | Height or depth in section/core (cm) | Latitude | Longitude | Sample type | Facies | Fraction modern | ¹⁴ C age (yr BP) | Uncert | Credible interval, calibrated using Marine20 and $\Delta R = -230 \pm 131$ years (yr BP; 95% CI) |
|----------------------------------|----------|------------------------|---|--------------------------------------|------------------------------------|--------------|-------------|----------|-----------------|-----------------------------|--------|--|
| 168125 | NOSAMS | FA-2-A | 13: FA-2 | 110 | N 21.284537° | W 71.694621° | Sediment | Facies 2 | 0.4981 | 5600 | 0.0015 | 5717–6346 |
| 168126 | NOSAMS | FA-4-A | 14: FA-4 | Not recorded | N 21.285907° | W 71.693341° | Sediment | Facies 2 | 0.5404 | 4940 | 0.0016 | 4949–5634 |
| 182382 | NOSAMS | LAC22-M-01 | No section, collected from beach facies | Not collected within section | N 21.29233° | W 71.68679° | Shell | Facies 1 | 0.9281 | 600 | 0.0018 | 29–529 |
| 182383 | NOSAMS | LAC22-M-02a | No section, collected from beach facies | Not collected within section | N 21.29286° | W 71.68583° | Shell | Facies 1 | 0.9477 | 430 | 0.0019 | 8–419 |
| 182384 | NOSAMS | LAC22-M-02b | | | | | Shell | Facies 1 | 0.9403 | 495 | 0.0020 | 12–458 |
| 182387 | NOSAMS | LAC22-M-02c | | | | | Shell | Facies 1 | 0.9414 | 485 | 0.0016 | 11–452 |
| 182388 | NOSAMS | LAC22-M-04a | 16: 05-SS | 46 | N 21.29341° | W 71.68465° | Shell | Facies 1 | 0.9507 | 405 | 0.0016 | 7–405 |
| 182389 | NOSAMS | LAC22-M-04b | | 46 | | | Shell | Facies 1 | 0.9452 | 455 | 0.0017 | 9–434 |
| 168138 | NOSAMS | WF-beach-B | 15: WOS | 0–10 cm interval | N 21.295513° | W 71.684439° | Shell | Facies 1 | 0.8579 | 1230 | 0.0017 | 588–1152 |
| 168137 | NOSAMS | WF-beach-A | | 0–10 cm interval | | | Shell | Facies 1 | 0.8953 | 890 | 0.0019 | 283–807 |
| 218539 | UCI Keck | West of (FA)-1C shell | No section, collected from beach facies | Not collected within section | N 21.28626° | W 71.69555° | Shell | Facies 1 | 0.8892 | 945 | 0.0017 | 328–867 |
| 218540 | UCI Keck | West of (FA)-1B shell | | | | | Shell | Facies 1 | 0.8986 | 860 | 0.0017 | 248–773 |
| CORE FROM ISLAND INTERIOR | | | | | | | | | | | | |
| 218527 | UCI Keck | VC03-030C shell frags | VC03 (Present <i>et al.</i> , 2021; Stein <i>et al.</i> , 2023) | –30 | N 21.29822° | W 71.70177° | Shell | NA | 0.8811 | 1015 | 0.0017 | 402–926 |
| 168139 | NOSAMS | VC03 – 40 | | –40 | | | Sediment | NA | 0.7967 | 1830 | 0.0016 | 1175–1796 |
| 218528 | UCI Keck | VC03-070 shell frags | | –70 | | | Shell | NA | 0.8598 | 1215 | 0.0016 | 574–1140 |
| 168140 | NOSAMS | VC03 – 80 | | –80 | | | Sediment | NA | 0.7696 | 2100 | 0.0016 | 1441–2131 |
| 218529 | UCI Keck | VC03 – 180 shell frags | | –180 | | | Shell | NA | 0.7303 | 2525 | 0.0015 | 1944–2667 |
| 168141 | NOSAMS | VC03-190 | | –190 | | | Sediment | NA | 0.7100 | 2750 | 0.0016 | 2222–2915 |
| MODERN BEACH SAND | | | | | | | | | | | | |
| | NOSAMS | BT1 | Modern beach sands (Trower <i>et al.</i> 2017) | Collected on modern beach | At eastern tip of Little Ambergris | | Sediment | NA | 0.8685 | 1130 | 0.0019 | 515–1049 |
| | NOSAMS | BT13 | | Collected on modern beach | 5.4 km west of BT1, along shore | | Sediment | NA | 0.8606 | 1210 | 0.0018 | 572–1133 |

measurement. Radiocarbon data are given as fractions of the modern standard (F_m) and as uncalibrated radiocarbon dates following the conventions of Stuiver & Polach (1977; Table 2).

To convert radiocarbon dates into calendar ages, the radiocarbon dates must be calibrated. The recommendations of DiNapoli *et al.* (2021) were followed for the calibration of ages presented in the main text, and alternative approaches were also considered (Table S2; Appendix S2; Reimer *et al.*, 2020) as sensitivity tests. A reservoir age correction of $\Delta R = -230 \pm 131$ years was first applied to all samples. This ΔR value is the regional pooled average of radiocarbon ages across the Lucayan archipelago (DiNapoli *et al.*, 2021), to which the Turks and Caicos Islands belong geographically. This value is consistent within uncertainty with the two closest reservoir ages offsets available in the Marine Calibration database to Little Ambergris Cay (<http://calib.org/marine/>; Reimer & Reimer, 2001; DiNapoli *et al.*, 2021): Cap Haitien (-145 ± 23 years) and Great Inagua (-232 ± 33 years), which are both *ca* 180 km away. Calibration was performed using the Marine20 radiocarbon calibration curve (Heaton *et al.*, 2020) and the R package Bchron (Haslett & Parnell, 2008). The credible age interval (95% confidence interval) is reported in cal yr BP (calendar years before present, where 0 year BP = 1950 CE, by convention; Godwin, 1962; Table 2).

The same approach was used to recalibrate previously published radiocarbon dates from Little Ambergris Cay (Table 2): shells from sediment core VC03 taken from the island's interior (Stein *et al.*, 2023) and modern beach sand (Trower *et al.*, 2018). Additionally, radiocarbon data for three samples of ooid sand from core VC03 are presented here for the first time (Table 2). The sedimentology of this core has been previously described (Present *et al.*, 2021). The credible age intervals associated with these samples are reported using the same process as described above.

Petrographic characterization

Petrographic thin sections were made from samples of lithified sediments. Prior to sectioning, samples were impregnated with epoxy under vacuum because they were friable and weakly cemented. Photomicrographs of these thin sections were made using a standard petrographic microscope and plane-polarized light.

RESULTS

Key geomorphological features

Little Ambergris Cay's interior is a tidal swamp dominated by mangrove patches and microbial mats, surrounded by a rim of lithified sediments. These sediments are occasionally exposed as outcrop at the modern shoreline or in erosional scours inland; elsewhere, they are covered by unlithified sands and scrub vegetation (Fig. S2). Tidal channels connect the island interior to the open platform, and the position of some of these channels appears to have been consistent over the last *ca* 150 years (Fig. 4). A kilometres-long ooid shoal (Lloyd *et al.*, 1987; Dravis & Wanless, 2008, 2017; Rankey *et al.*, 2008; Trower *et al.*, 2018) extends to the west from the tip of the island. The island's shape and east–west orientation is aligned with the dominant direction of the trade winds (Wanless *et al.*, 1989; Dravis & Wanless, 2008, 2017; Trower *et al.*, 2018). In general, the north coast of the island includes thicker outcrop exposure at the coastline (Fig. 2) and is higher topographically (Stein *et al.*, 2023). The southern coast of the island tends to have thinner outcrop exposure (Fig. 2) and to be topographically lower. The south-eastern shore of the island is dominated by a strandplain covered by scrubby vegetation. Hurricane Irma eroded portions of this strandplain in 2017, exposing limited outcrop in the island interior (Jamison-Todd *et al.*, 2020). An important exception to this overall pattern of northern thick exposures and southern thin exposures is the south-east-trending linear feature at the island's southern extreme, which is referred to as the southern lineament. The southern lineament includes the thickest outcrop exposures on the island.

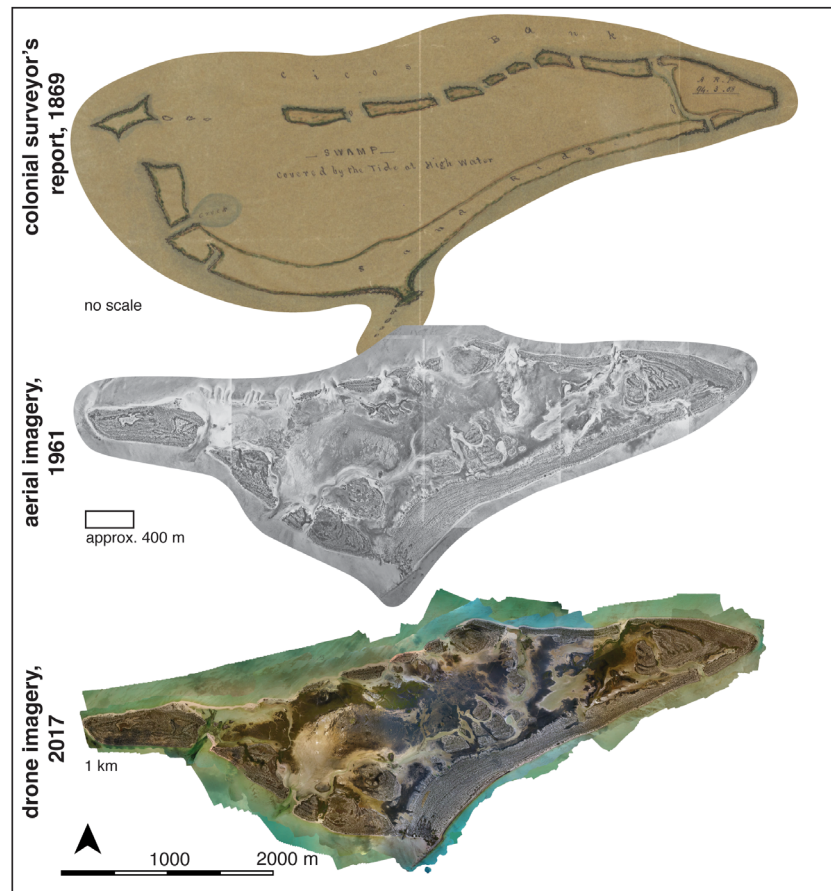
Facies analysis

There are three facies present in the lithified sediments of Little Ambergris Cay. All rocks studied are limestone, and any post-depositional tilting, deformation or compaction of strata, if present, is subtle.

Facies 1: Fossiliferous, planar to seaward dipping grainstone

Description. This facies is characterized by planar to seaward-dipping beds (Fig. 5A to H).

Fig. 4. Historical documents show that many features of Little Ambergris Cay, such as the position of tidal channels and the southern lineament, have persisted since at least the 19th century. Top: map from a report by Colonial Surveyor Wynns to Colonial Governor Grant regarding the lease of Little Ambergris Cay, 1869. From The National Archives (UK). Middle: archival aerial imagery of Little Ambergris Cay in January 1961 from the National Collection of Aerial Photography (Edinburgh, Scotland). Bottom: drone imagery collected in 2017.



Faint parallel lamination is sometimes visible. It frequently contains shell material (Fig. 5E to H), keystone vugs (Fig. 5F) and ripples (Fig. 5C). It can also contain burrows. Grains are medium sand-sized. Framework grains are predominantly ooids, but skeletal grains, including *Halimeda* plates, foraminifera and shell fragments, are also present. Meniscus and pendant cements are observed in petrographic thin section (Fig. 6A and B). Strata belonging to this facies are generally more poorly sorted and coarser-grained than those from facies 2. The skeletal material found in facies 1 includes bivalves, gastropods, corals and calcareous algae. In some locations, shell-rich deposits are present in this unit (Fig. 5G), although in other locations, fossils are rare or absent (for example, at the north-eastern edge of the island, at section 1, EN2-J18). Arcoid bivalves are especially abundant; these are often present, even in otherwise fossil-poor exposures (Fig. 5H). They are typically found as intact, disarticulated valves, but in rare instances remain articulated. Carbonate concretions associated

with mangrove prop roots occur in this facies especially along the west end of the island (Fig. 5E).

This facies is best preserved along the southern coast of the island, especially the south-western coast. At section 10, WBBRO, at least three packages of prograding deposits are preserved. Sedimentary beds stack laterally seaward (Fig. 5A and B). These packages include the inflection point where planar bedding 'rolls over' to seaward-dipping bedding (Fig. 5A and B); other deposits with this rollover are found elsewhere along the southern coast (Fig. 5D). On the north coast of the island, it is more difficult to identify this facies in outcrop; northern exposures are less shell-rich, and the beds containing this facies are often covered by rubble or not exposed. On the north shore of the island, no prograding deposits are preserved, and exposure of this facies is often limited to the top of a bed marked by scattered bivalves and occasional keystone vugs. This facies is also preserved in the island interior, both on the north side of the

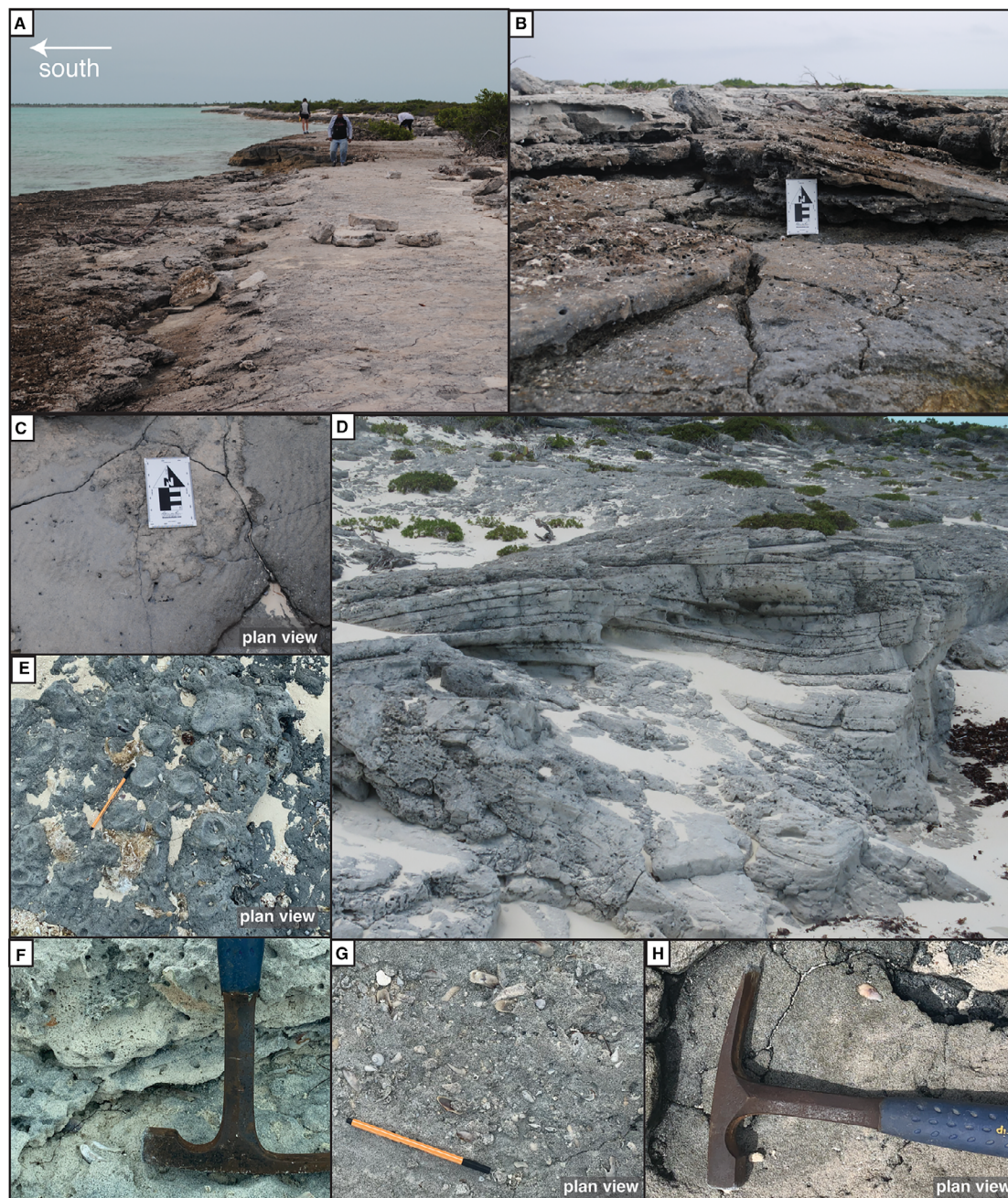


Fig. 5. Key characteristics of the fossiliferous, planar to seaward dipping grainstone facies. (A) At section 10, WBBRO, a series of deposits prograde to the south. Shells and keystone vugs characterize these deposits. Researchers for scale, *ca* 1.8 m tall. (B) The inflection point in a prograding deposit where bedding dip direction changes from horizontal to seaward dipping. The stacking, shingling pattern of the prograding deposits can be seen here. From section 10, WBBRO. (C) Wave ripples on a bedding surface. From section 10, WBBRO. (D) Horizontal to seaward-dipping grainstone overlain by low-amplitude aeolian deposits. View is landward. From south coast of island. (E) Concretions along mangrove prop root casts within shell-rich bed from facies 1. Pen is 18.1 cm long. From south-western-most point of the main part of Little Ambergis Cay, before the major western tidal channel, coordinates N 21.29434° W 71.71387°. (F) Both keystone vugs and burrows are present within the foreshore facies. Rock hammer for scale, *ca* 30 cm long. From section 9, WBB2. (G) This facies includes a diverse faunal assemblage, including bivalves, molluscs, green algae and coral. Arcoid shells are particularly abundant and can be found articulated, though rarely. Dense, channelized fossil-rich deposits can be found perpendicular to the shore in some areas. Pen is 18.1 cm long. Near section 10, WBBRO. (H) The foreshore facies, where it is fossil-poor, is dominated by arcoid bivalves. Rock hammer for scale. From section 3, 15-C2.

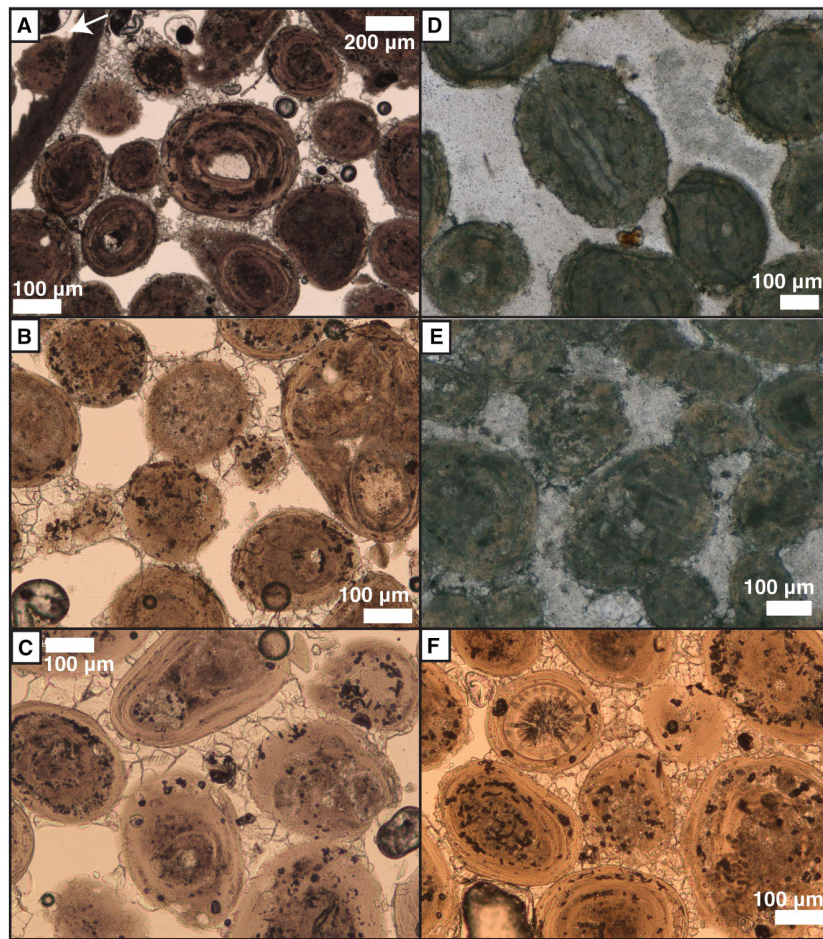


Fig. 6. Photomicrographs of rock samples from Little Ambergris Cay. (A) Meniscus and pendant cements in facies 1, which is dominated by ooids. Geopetal structure (grains cupped in shell) in top-left corner of image, marked with arrow. Way up is to the left. Sample collected near section 10, WBBRO. Plane-polarized light. (B) Meniscus cements, ooids and a compound coated grain from facies 1. Sample collected near section 10, WBBRO. Plane-polarized light. (C) Grains and cements from facies 2. Micritization of grains and meniscus cements visible. Sample collected near section 10, WBBRO. Plane-polarized light. (D) Sample of facies 2 from the southern lineament, showing finer grain size, more cement formation and poorer preservation of grain internal structure than (F). Sample collected at section 14, 8/6 FA-4. Plane-polarized light. (E) Intergranular blocky cement within facies 3. Sample collected near section 10, WBBRO. Plane-polarized light. (F) Sample of facies 2 from a coastal section on the lithified rim of Little Ambergris Cay, showing coarser grain size and fewer cements than (D). Sample collected at section 3, 15-C2. Plane-polarized light.

island up a tidal channel (section 4, 14-C2) and at scour pits eroded during Hurricane Irma (section 15, WOS; Fig. 7A).

Interpretation. Given its abundant shell material, wave ripples and bedding relationships, it is interpreted that this facies was deposited in a foreshore environment. Where keystone vugs are present, deposition within the upper swash zone of a beach can be more precisely identified. The presence of carbonate concretions associated with mangrove prop roots (Fig. 5E), which are largely subaerial, support deposition

of this facies in shallow water. The meniscus and pendant cements found within this facies are consistent (Fig. 6A and B) with cementation in the vadose zone. Where it is exposed, this facies is always the lowest unit in a stratigraphic section.

The rollover point preserved within packages of this facies is interpreted as marking the transition between a flat-lying beach berm and seaward-dipping beds, with seaward progradation and growth of the island recorded as lateral shingling.

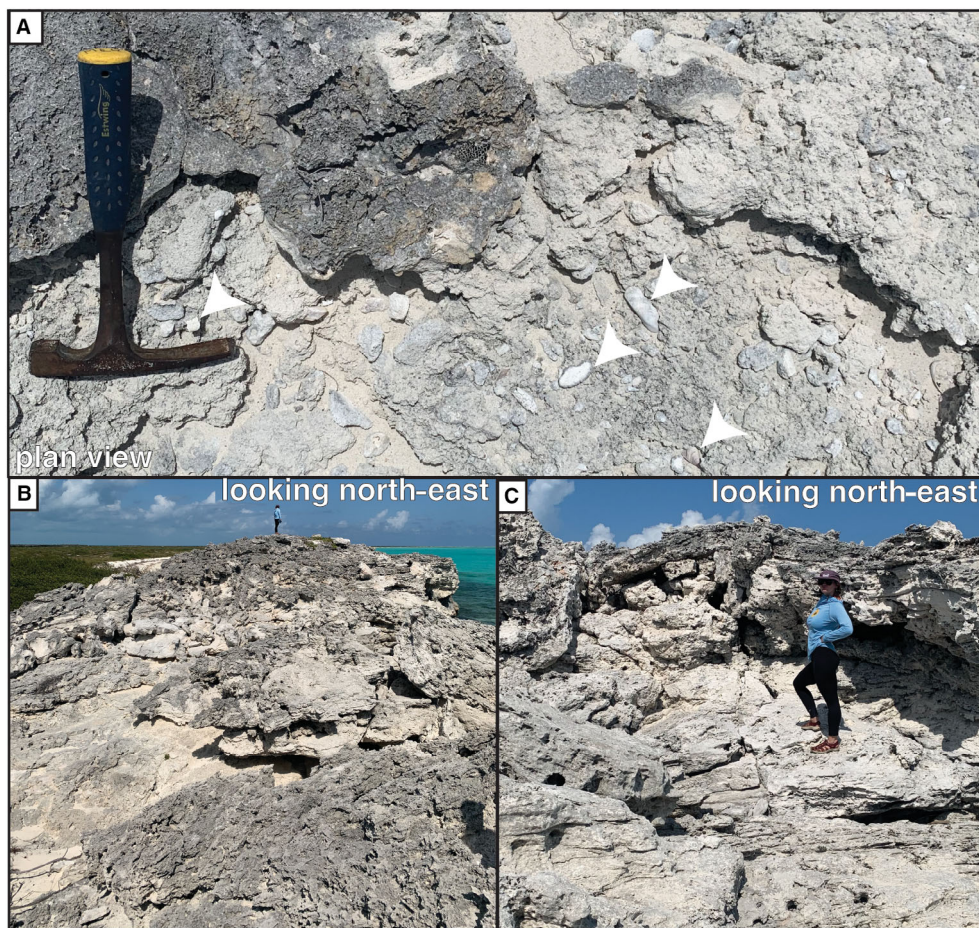


Fig. 7. Other locations around the island. (A) Shell-rich beds exposed at section 15, WOS. Scour pits generated during Hurricane Irma in 2017 expose shell-rich beds which are capped by aeolian dunes and terrestrial flora. The location in this photograph is approximately 175 m from the modern coastline. The faunal assemblage present is comparable to that observed in coastal exposures of shell-rich intertidal facies. Arrowheads point to shells. Hammer for scale, *ca* 30 cm long. (B) Vertical opening-mode fractures run along the southern lineament, oriented with the overall south-west trend of the feature. Geologist for scale, *ca* 1.8 m tall. (C) Another location in the southern lineament where vertical opening-mode fractures are visible. Geologist for scale, *ca* 1.8 m tall.

Facies 2: Trough cross-stratified, well-sorted grainstone with root and stem casts

Description. This facies is marked by decimetre-scale to metre-scale trough cross-stratification and compound cross-stratification, abundant root casts and traces, and pinstripe lamination (Fig. 8). Rarely, it can contain coarser-grained layers with rounded, granule to coarse-sand-sized skeletal fragments. Grain size more typically ranges from fine to very fine sand. Ooids are the predominant grains in this facies, though *Halimeda* plates are also present; the grain composition is broadly similar to that of facies 1, but with the absence of foraminifera. This facies always occurs above facies 1 where both are present and, in some locations, dune

forms are fully lithified as fossil bedforms and can be seen prograding over beds of facies 1 (section 5, WC2).

This facies is best exposed along the north coast of the island (Fig. 2) in coastal outcrops 2 to 3 m tall. It is also present, but thinner – typically a poorly exposed unit of a few decimetres – along the southern coast (Fig. 3) and it underlies the strandplain at the south-east coast of the island (Fig. 1; Fig. S2). A south-west-striking feature located on the southern shore of the island (Fig. 1) and documented by sections 12 (8/6 FA-3), 13 (8/6 FA-2) and 14 (8/6 FA-4) (Fig. 3) is an important exception to this generalization (Fig. 8A to E). This location is referred to as the southern lineament (Fig. 8E). Here,

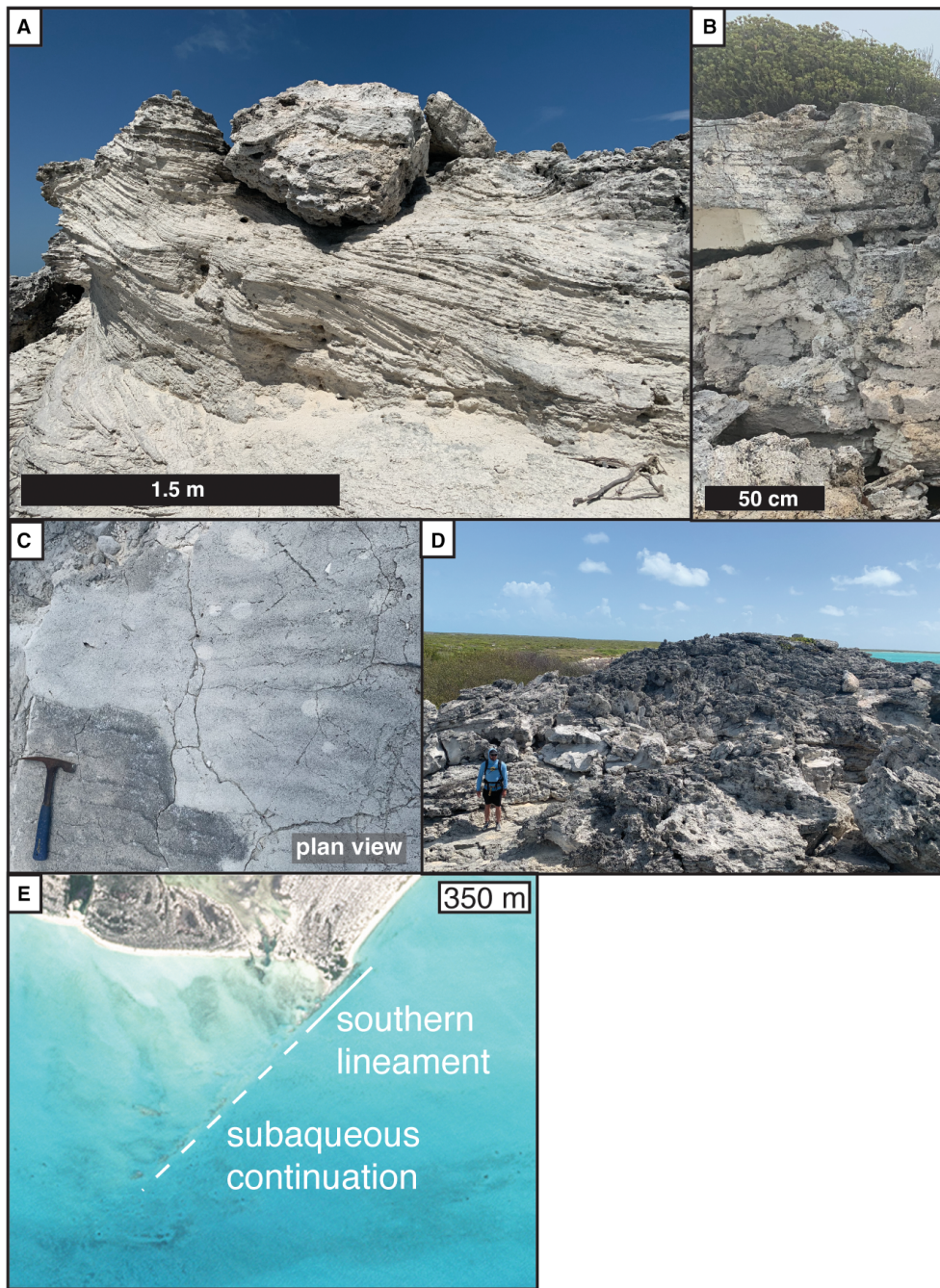


Fig. 8. Key characteristics and features associated with facies 2, trough cross-stratified, well-sorted grainstone with root casts, on Little Ambergris Cay. (A) Large-scale trough cross-bedding, often larger than the outcrop. Pin-stripe lamination also present. From the southern lineament on the southern coast of the island. At this location, the scale of cross-bedding and height of outcrop is larger than seen elsewhere on the island. (B) Aeolianite with root casts visible near top. Photograph taken near section 3, 15-C2. (C) Wind ripples on bedding surface at top of dune. On north-east coast of island. Ripples consistent with the prevailing easterly wind direction on Little Ambergris Cay. (D) The height of the aeolianites at the southern lineament is greater than seen elsewhere on the island. Researcher is 183 cm tall. (E) The southern lineament continues subaqueously for more than a kilometre to the south-east. Imagery from Planet (Global Quarterly Basemap, First Quarter 2023; imagery date 16 March 2023).

eroding pinnacles form a spur that extends into the sea. The same facies exposed in other coastal sections has a coarser grain size (Fig. 6C) than at the southern lineament; rocks at the southern lineament are also more indurated and the internal structure of grains is more poorly preserved (Fig. 6D and E). In contrast to the largely east–west structure of the island, the southern lineament has a clear north–east to south–west linear trend. Satellite imagery of Little Ambergris Cay shows that this feature extends for more than a kilometre subaqueously (Fig. 8E, imagery accessed from Planet Team, 2022). The southern lineament also contains opening-mode fractures which run parallel to the overall trend of the feature and extend for tens of metres. These fractures do not follow bedding, nor do they widen towards the surface or show evidence for dissolution (Fig. 7B and C). No displacement is observed across these cracks.

Interpretation. This facies is interpreted as reflecting aeolian reworking of ooid sand sourced from nearby beaches and redeposition in subaerial sand dunes up to several metres in height. The ooid sand was reworked from beach deposits. The southern lineament and its relationship to the coastal exposures of this facies is discussed in greater detail in the section *Age and correlation of the southern lineament*, and suggest that differences in their outcrop character, orientation, induration, grain size and preservation are consistent with a separate origin for this feature, an interpretation further supported by radiocarbon data.

Facies 3: Cobble to boulder rudstone

Description. Cobble to boulder rudstone, dominated by occasionally imbricated clasts of ooid grainstone within an ooid grainstone matrix (Fig. 9A to D), make up this facies. The clasts are sourced from facies 1 or 2. Clasts are coherent, with clear edges, and angular. Shells, including adult queen conch, are incorporated in some localities. The lateral extent of any single occurrence of this facies is typically limited to a metre or two at most, and occurrences form distinct metre-scale mounds and piles. Stratigraphically, this facies can occur at any level and can extend to sea level. It is better cemented in occurrences near the modern shoreline and occurs on both the northern and southern shores.

Most clasts incorporated into the rudstone are carbonate grainstone clasts or shells, but some

have an anthropogenic origin. Human detritus including glass bottles, exotic rock clasts, hunted conch and metal fragments are incorporated into the cemented rudstone matrix.

Interpretation. This facies records the erosion, transport and relithification of locally sourced clasts. The structural coherence and clear edges of the incorporated clasts indicate that they were sourced from pre-existing sediments and were lithified before erosion. The clasts' size, angularity and similarity to nearby rock all indicate that these clasts were not transported far before redeposition. Better cementation of this unit in occurrences near the modern shore (Fig. 6F) is likely linked with processes of carbonate beachrock formation.

At section 12, 8/6 FA-3, a quartzite boulder is incorporated into a conglomerate encrusting an outcrop. Because there is no silicate rock exposed in the Turks and Caicos Islands, this boulder is likely anthropogenic debris, perhaps related to historic or recent construction, ship's ballast, or prehistoric tool manufacture. However, the possibility of transport by non-human mechanisms like kelp (Emery & Tschudy, 1941; Garden & Smith, 2015) or driftwood (Emery, 1955) cannot be eliminated. The colourless, bubble-free glass and externally threaded screw-tops of bottles found in this facies indicate that they were manufactured no earlier than the 20th century (Lindsey, 2021). The presence of these bottles demonstrates that lithification is occurring over timescales of centuries or decades, at most, on Little Ambergris Cay.

Field observations after Hurricane Irma in 2017 confirmed that hurricane-related waves and storm surges contribute to the brecciation of the lithified rim (Stein *et al.*, 2017, 2023; Jamison-Todd *et al.*, 2020). Rather than being formed in a single event, these localized conglomerates have probably been generated throughout the island's history.

Radiocarbon data

Consistent with previous reports indicating a Holocene age for Little Ambergris Cay (Orzechowski *et al.*, 2016; Dravis & Wanless, 2017; Stein *et al.*, 2023), all dates measured in this study are Holocene. Ages for each sample are shown as a continuous credible age interval with a 95% confidence interval (Figs 2 and 3; Table 2). No evidence for Pleistocene rock exposed in outcrop on Little Ambergris Cay was found in this study, and no shell samples from



Fig. 9. Key characteristics of facies 3, cobble to boulder conglomerate, present on Little Ambergris Cay. (A) and (B) Reworked boulders and cobbles in conglomerate. Rock hammer for scale, *ca* 30 cm long. (A) is a locality on the north-west shore of the island; section 5, WC2 is the closest measured section. (B) is a locality on the south-west shore of the island between sections 9 (WBB2) and 10 (WBBRO). (C) Some conglomeratic units contain human debris, including glass bottles like this one, as well as metal fragments, asphalt and hunted conch shells. The bottle's externally-threaded lid and its transparent, bubble-free glass indicate a date of manufacture no earlier than the 20th century. Location is the south-east shore of the island, coordinates N21.29988° W71.67142°. Pen for scale is *ca* 15 cm long. (D) Some conglomeratic units are also fossiliferous. A juvenile queen conch is shown in a conglomerate here. From section 10, WBBRO.

lithified sediments now exposed at the surface are older than 1400 cal yr BP, regardless of what calibration scheme is used (Table 2; Table S2). The oldest samples are carbonate aeolianite taken from the southern lineament, which return calibrated credible age intervals in the mid-Holocene, thousands of years older than any other samples from the island.

Shells with stratigraphic context yield age relationships consistent with the predicted stacking or depositional order. In general, shells sampled from the same bed yield overlapping calibrated credible age intervals. Such an age relationship suggests that deposition of the associated bed is reasonably well-constrained by the ages of the shells inside. The exception are shells from section 15, WOS; the ages of these shells are close but do not overlap. This shell-rich, chaotic bed may record a high-energy event

that reworked and deposited both older and contemporary shells; the depositional age of the containing unit is best constrained by the age range of the younger shell.

Calibrated credible age intervals for radio-carbon samples from previous work on Little Ambergris Cay (Table 2) are also included. VC03 is a previously described sediment core from the interior of the island (Present *et al.*, 2021; Stein *et al.*, 2023). The stratigraphically lowermost dated shell in this core dates to 1944 to 2667 cal yr BP, which is older than any shell found in outcrop. In this core, dated sediments and shells obey stratigraphic superposition with respect to samples of the same type, but ooid sands are anywhere from a few hundred to a thousand years older than stratigraphically proximate shells in the same section. Similar offsets between sediment ages and shell ages are seen at section 2,

CL. Ages from modern sand on the shore of Little Ambergris Cay from Trower *et al.* (2018) are recalibrated here using the age calibration scheme described above (Table 2).

DISCUSSION

Accuracy and precision of radiocarbon data

Limited information on local marine reservoir effects in the Ambergris system and on the Caicos Platform more broadly limit the accuracy and precision of radiocarbon ages presented in this study. Firstly, no local radiocarbon reservoir age correction exists for the Turks and Caicos Platform, and prior work has shown large spatial variability in ΔR across the Caribbean (DiNapoli *et al.*, 2021). Secondly, the necessity of a marine reservoir correction in the Ambergris system may not exist if local platform waters are in equilibrium with the atmosphere. To explore these possibilities, radiocarbon ages under different sensitivity tests are also reported (Table S2; Appendix S2). The issues explored in the sensitivity test – local reservoir age correction and the equilibrium of Ambergris waters with the atmosphere – have important implications for the accuracy and precision of this study's reported dates and future dates from the Turks and Caicos Islands. Indeed, a scenario assuming equilibrium between Ambergris waters and the atmosphere shifts calibrated ages several centuries older than reported in Table 2 (Table S2; Appendix S2). These concerns are particularly relevant for archaeological, sea level and palaeoclimatic studies, and can only be conclusively resolved by future work establishing a reservoir age correction for the Caicos platform or Ambergris system. Some lithified shell samples (current study) are <603 year BP and therefore too young for calibration with the Marine20 calibration curve. Nevertheless, under all sensitivity tests, the broad conclusion that all samples from Little Ambergris Cay are Holocene in age remains robust.

Age, correlation and recent, rapid progradation of Little Ambergris Cay's lithified rim

Shell ages from across the island help to establish a minimum age for the lithified rim of the island (Figs 2 and 3; Table 2):

- The lower shell from section 11, 8/9 BB-5 on the southern coast, is dated 578 to 1145 cal yr BP.
- The younger shell preserved *in situ* in the southern island interior at section 15, WOS, dates the unit to no older than 283 to 807 cal yr BP.
- The younger shell from the northern interior at section 4, 14-C2, suggests deposition at 537 to 1081 cal yr BP.

Shell-bearing units may incorporate older shells; thus these are most conservatively interpreted as maximum age constraints, still supporting exclusively Holocene ages for exposed, lithified sediments on Little Ambergris Cay. Taken together, the above data is interpreted as supporting deposition in a foreshore environment on both the northern and southern coasts of the island by 500 cal yr BP and perhaps as early as 1000 cal yr BP. Such a scenario is consistent with the modern geometry of the island, with an external rim of the island protecting a low-energy, restricted interior lagoon. These data support identification of the regional equivalent of Little Ambergris Cay's lithified sediment rim, except for the southern lineament, as the Hanna Bay Member of the Rice Bay Formation (Fig. 10), an intertidal to aeolian unit that dates to the late Holocene, described across the Lucayan archipelago (Myroie & Carew, 1995; Kindler & Hearty, 1996; Myroie *et al.*, 2008; Godefroid, 2011).

Multiple observations indicate that lithification occurs rapidly on Little Ambergris Cay. The presence of anthropogenic debris, including glass bottles, exotic rock fragments and metal, within fully lithified rudstones (Fig. 9C) demonstrates that lithification can occur on human timescales. In some locations along the coast, radiocarbon dates from lithified shells at the modern shoreline are also consistent with recent deposition and lithification (Figs 2 and 3; Table 2). The rapid lithification of carbonate beachrock over intervals of decades to years has been documented elsewhere (Wiles *et al.*, 2018; Falkenroth *et al.*, 2022) – even on timescales of weeks to months (McCutcheon *et al.*, 2016, 2017). Early synsedimentary vadose lithification, evidenced by meniscus and pendant cements in samples from the island (Fig. 6A to E) stabilizes sediment on Little Ambergris Cay, and has been observed elsewhere in the Bahamian archipelago (Halley & Harris, 1979).

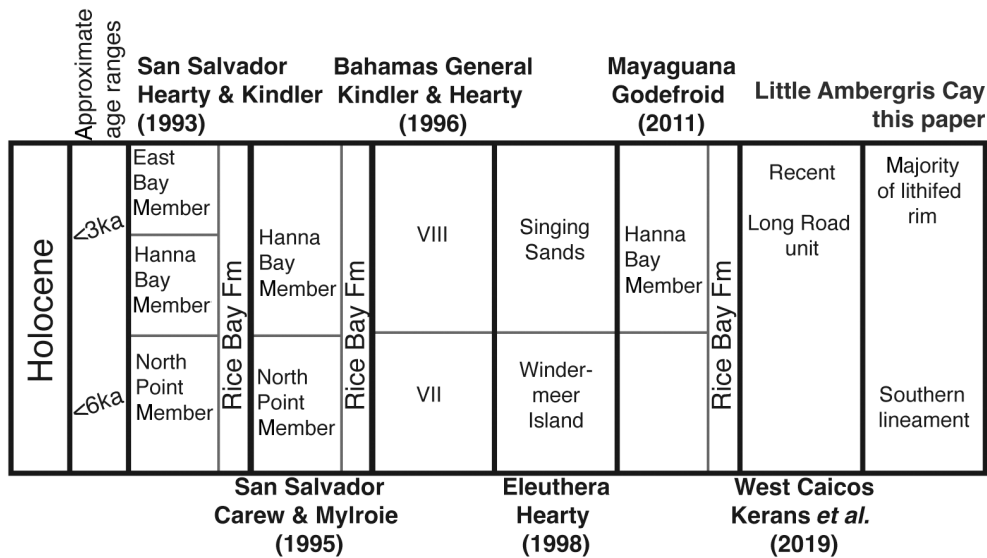


Fig. 10. Stratigraphic correlation across the Holocene of the Lucayan archipelago, including Little Ambergris Cay. Modified after Kerans *et al.* (2019).

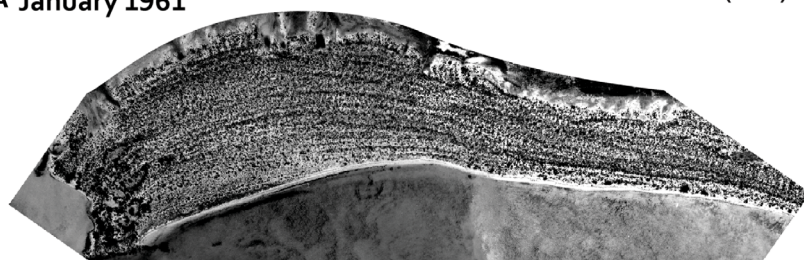
Data from this study indicates lateral progradation and growth of the island over the last millennium. Age differences in shells found in inland exposures compared to those found on coastal exposures (for example, section 15, WOS, versus section 16, 05-SS; or section 4, 14-C2, compared to section 3, 15-C2) show older shells within the island interior and younger ages on the modern shore, consistent with lateral growth of Little Ambergris Cay. Sedimentological evidence of this growth is preserved at section 10, WBBRO, where prograding, shingling foreshore deposits record the southward growth of the island. Finally, this growth is also seen in the observational record: comparison of aerial imagery of Little Ambergris Cay from 1961 to 2016 documents progradation on the southern shore of the island of about 20 m at its maximum (Fig. 11). The strandplain on the southern shore of the island records the island's accretion and growth to the south, and it tapers northward, from a maximum width of *ca* 500 to *ca* 50 m.

The implied rates of lateral progradation vary between the southern and northern shore. Section 15, WOS, is located about 175 m inland from the island's modern southern shore. If deposition of the shell-bearing unit exposed there falls within the credible age interval of the dated younger shell (Table 2), lateral progradation to the modern coastline averaged between 22 and 62 cm/year. The oldest

constraints produced in a sensitivity test yield rates close to 20 cm/year (Table S2). This range is consistent with a comparison of aerial imagery from 1961 and 2016 which suggests lateral progradation on the southern shore at a maximum rate of about 35 cm/year. On the northern shore of the island, section 4, 14-C2, is exposed at a tidal channel about 60 m from the modern shore. If the depositional age of this unit is constrained by the younger of two dated shells within it (Table 2), progradation has averaged 6 to 11 cm/year. (Using the oldest constraints produced in a sensitivity test yields rates of 5 to 6 cm/year; Table S2.) These calculated rates of progradation are comparable or an order of magnitude lower than rates of progradation determined for the Holocene Persian Gulf (Lokier & Steuber, 2008). Both the strandplain on the south-east coast of the island and the preservation of shingled foreshore packages at section 15, WBBRO, are interpreted as recording this southward progradation.

The island's northern and southern shores exhibit systematic differences in the exposure of the lithified rim. On the north, erosion has exposed the interiors of aeolian sand dunes 2 to 3 m in height. This is consistent with observations made in the wake of Hurricane Ike (2008), when erosion was noted along the northern shore of the island (Dravis & Wanless, 2017). Lower rates of net progradation to the north may reflect the impact of such erosion. In the south,

A January 1961

modified after Stein *et al.* (2023)

B June 2016

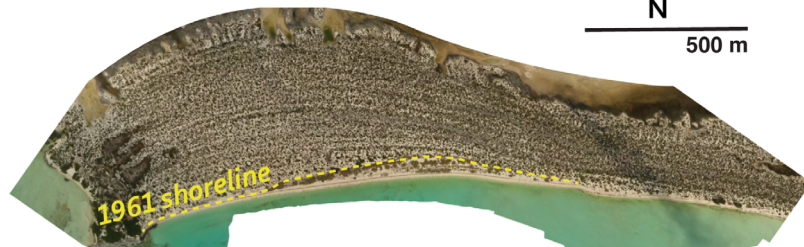


Fig. 11. Archival aerial imagery of Little Ambergris Cay in January 1961 from the National Collection of Aerial Photography (Edinburgh, Scotland). The same area of Little Ambergris Cay in July 2016 is shown below, with the georeferenced 1961 shoreline traced in yellow. Previously published in Stein *et al.* (2023).

foreshore units are exposed with less outcrop exposure of aeolianites (except at the southern lineament, which we argue below is a separate case; Fig. 3). Aeolian facies are present on the southern coast; the strandplain present on the south-east coast of the island is made up of lithified sand dunes, but they are not well-exposed in outcrop.

The youngest shells are found along the modern coastline on both the northern and southern coasts (Figs 2 and 3; Table 2). Older shells are found within the island interior (Table 2). These data support the conclusion that Little Ambergris Cay has grown by both northward and southward progradation over the last millennium. It is more difficult to detect a signal of east–west growth in this dataset.

The recent growth and progradation of Little Ambergris Cay contrasts with recent work showing shoreline retrogradation on Andros Island in recent decades (Wu *et al.*, 2021). Both Little Ambergris Cay and Andros Island are part of the Lucayan archipelago, and both have experienced similar recent sea-level rise. Both are lagoonal islands dominated by microbial mats and mangrove thickets. The difference between Little Ambergris Cay's progradation and the retrogradation of the Andros Island shoreline is attributed to differences in sediment supply. The Ambergris system produces abundant ooid sand, and sediment supply outpaces sea-level rise; in contrast, local production of mud on Andros Island is insufficient to balance sea-level rise.

Age and correlation of the southern lineament

Aeolianite sediment samples from the southern lineament are dated to credible intervals of 5717 to 6346 cal yr BP and 4949 to 5634 cal yr BP: thousands of years older than any shell sample on the island (Fig. 3; Table 2). However, the radiocarbon ages of aeolianite carbonate and shells are not comparable without some caveats.

Firstly, radiocarbon ages from ooids are inevitably averaged ages that do not correspond to a specific precipitation event. The measurement of several individual sand grains is required to produce a radiocarbon age and the resulting age is therefore averaged across several grains. Sequential dissolution of ooids shows that different layers have distinct radiocarbon ages, becoming older towards the centre of the grain (Beaupré *et al.*, 2015). Therefore, even the radiocarbon age of a single grain would average over the formation history of the grain. This time-averaging characteristic of ooid radiocarbon ages is distinct from the radiocarbon age of a shell, which corresponds to the lifespan of a single animal.

Secondly, radiocarbon dates from aeolianites constrain precipitation of the carbonate grains in a marine environment, not aeolian deposition directly. It is possible that carbonate sand grains might precipitate in a subaqueous shoal setting and then spend substantial time in either subaqueous and/or subaerial modes of transport, before being buried in an aeolian dune. However, only the timing of subaqueous

precipitation can be dated by radiocarbon. By contrast, when a shell is found in a peritidal unit, one interpretation is that the death of the biomineralizing organism provides an approximate equivalent for depositional age (although reworking of shell material is always possible; Flessa *et al.*, 1993).

Interpretation of the southern lineament as the most ancient feature on Little Ambergris Cay must be tempered by these cautions. However, other evidence is consistent with the suggestion that the lineament is the oldest part of Little Ambergris Cay.

Firstly, the overall geometry and trend of the southern lineament contrast with all other features on the island. Its north-east – south-west trend, which extends for more than a kilometre subaqueously (Fig. 8E), is unlike any other lithified feature on the island. This trend does not align with the dominant east to west direction of wind or sediment transport (Fig. 8E). Nor does this trend align with sedimentary structures or bedding within the dunes; it appears to be the result of erosion. Evidence for non-aeolian deposition in the southern lineament was not found in this study despite repeated searching, although this may be due to extensive erosion in the tidal range. The scale and size of the dunes at the southern lineament are also different from smaller aeolian dunes elsewhere on the lithified rim (compare Figs 2 and 3). The grain sizes of sediment in these dunes, their induration and the preservation of grain interior structures are also distinct (Fig. 6D and E). These observations are consistent with different origins for these features. Limited exposures of aeolian dunes on the southern coast of the island also further highlight the distinctiveness of the southern lineament.

Secondly, previous studies examining the radiocarbon ages of carbonate sediment in the Turks and Caicos Islands (Lloyd *et al.*, 1987; Trower *et al.*, 2018) provide context for interpreting the radiocarbon ages of the southern lineament aeolianites. Samples of modern foreshore sand from the beaches of Little Ambergris Cay yield credible age intervals of 515 to 1049 cal yr BP and 572 to 1133 cal yr BP (Table 2). At least in the modern system, then, beach sand – which was the ultimate source of sand for the aeolian system that deposited the southern lineament – is substantially younger than sediment from the southern lineament. This suggests that several thousand years have passed since southern lineament sediment was beach

sand, though it is noted that this time could have been spent as either lithified or unlithified sediment in an aeolian system. Another study of Holocene aeolian dunes in the Turks and Caicos Islands found that the radiocarbon ages of prograding dunes obeyed stratigraphic superposition and were consistent with the dunes recording near-depositional ages (Lloyd *et al.*, 1987). The single exception was in a sample with significant ingrowth of younger calcite cement (Lloyd *et al.*, 1987). Finally, results from core VC03 and section 2, CL (Fig. 2), suggest that where shells and ooid sand occur in stratigraphic superposition, ooid sands will be consistently older than associated shells by several centuries – but not by thousands of years. This indicates that aeolianite ages do track depositional age within a lag of a few centuries; and dated sediment from an aeolian dune on the north shore of the island at section 2, CL, is dated at 491 to 1019 and 482 to 1008 cal yr BP in age (Table 2) – not mid-Holocene. Taken together, these data support the idea that the southern lineament sediment is thousands of years older than modern beach sand and that the radiocarbon ages of aeolianites are not widely decoupled from their depositional ages. Therefore, the radiocarbon ages of the southern lineament support its greater antiquity relative to other features of Little Ambergris Cay.

The scale and extent of the southern lineament dunes (Fig. 8B and C), and their modern-day fragmentary nature, imply the existence of an ancient and more widespread aeolian dune field. This *ca* 5000 cal yr BP aeolian dune unit is correlated with the North Point Member described from San Salvador, an early transgressive aeolian deposit, and elsewhere across the Lucayan archipelago (Fig. 10). The North Point Member dates to *ca* 3000 to 6000 year BP; it contains aeolian facies which extend to 2 m below modern sea level, and no intertidal facies (White & Curran, 1988; Hearty & Kindler, 1993; Mylroie & Carew, 1995; Kindler & Hearty, 1996; Mylroie *et al.*, 2008). On San Salvador Island in The Bahamas, it frequently occurs as sea stacks (Mylroie & Carew, 1995, fig. 4). The southern lineament exposures share these characteristics with the North Point Member.

Why the eroding remnants of the southern lineament have such a clear orientation apparently decoupled from wind direction, sediment transport or sedimentary structures within the dunes remains an open question. No displacement or tilting that strongly supports a structural

explanation was observed. This feature has likely been an important barrier to sediment during the nucleation and growth of the modern island. The prograding strandplain east of the southern lineament suggests that this feature currently promotes sediment deposition along the southern coast of the island by acting as a wave and sediment break.

Model for island growth and evolution

Observations are integrated here to articulate a model for the nucleation, formation and growth of Little Ambergris Cay. Historical documents from 1961 and 1869 show that the island has had its present form, a rim surrounding a tidal lowland, since at least the 19th century (Fig. 4). Previous interpretation of the Ambergris Cay system noted that Little Ambergris Cay sits in the lee of Big Ambergris Cay, and suggested that the island formed as a tombolo, an accretion of sand in the lee of a larger island (Dravis & Wanless, 2017; Stein *et al.*, 2023). The intensity and persistence of the trade winds on the Caicos platform undoubtedly make them important in any consideration of long-term landscape evolution, and the sedimentology and geochronology of these units can now be integrated to deliver a more detailed model for island growth and evolution.

The geology of Big Ambergris Cay has not been systematically described, but its high relief, its well-developed system of caves, and the extensive induration of exposed outcrop on the island interior have been noted. All of these features are consistent with an inferred Pleistocene age (Dravis & Wanless, 2017) and the presence of Big Ambergris Cay is likely an important boundary condition on the formation of Little Ambergris Cay, given its upwind location. No evidence has been found in outcrop for a Pleistocene precursor of Little Ambergris Cay, so island growth history starts in the early Holocene, when Big Ambergris Cay had no sister island (Fig. 12A) and the platform was exposed. In the early to mid-Holocene, sea level transgressed on the Caicos Platform and, as the platform flooded, carbonate sediment was produced locally and reworked by wind, creating the aeolian deposit now exposed in the southern lineament (Fig. 12B); the North Point Member (White & Curran, 1988; Hearty & Kindler, 1993; Mylroie & Carew, 1995; Mylroie *et al.*, 2008) is its regional, early transgressive aeolianite equivalent on San Salvador. At the time of deposition,

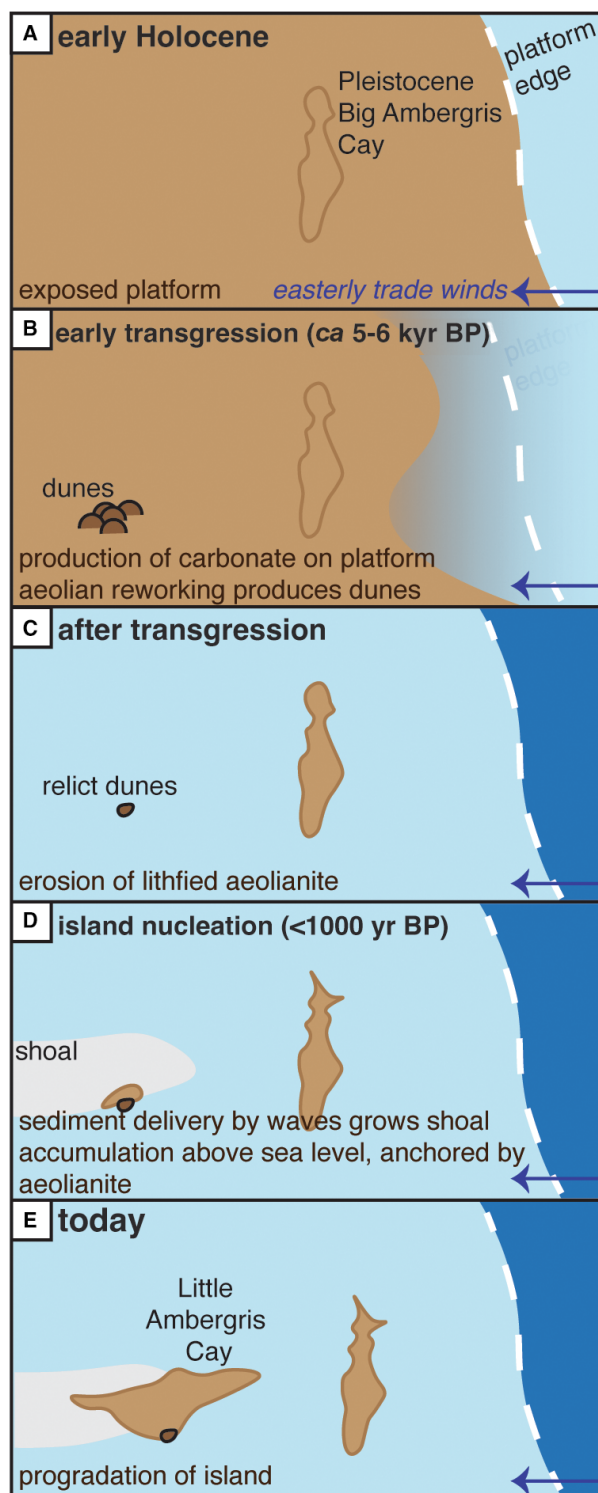


Fig. 12. Illustrative model for growth of Little Ambergris Cay based on the data presented here.

sea level was lower (3 to 6 m in the Bahamas; Khan *et al.*, 2017) than modern. This dune field was subsequently lithified and eroded, but part

of it – what would become the southern lineament – remained (Fig. 12C).

As sea level continued to rise and reached close to its modern level during the late Holocene, sediment production within the Ambergris Cay system increased (Fig. 12C). Shallow, wind-agitated water and precipitation of aragonite resulted in the development of the Ambergris ooid shoal (Fig. 12D). Overall, the system is controlled by the westward, wind-driven movement of waves and sediment driven by the easterly trade winds. As at other locations in the Lucayan archipelago, shoal development results in subaerial exposure of sediments (Harris, 1979) which then cement subaerially, forming a pavement or lithified surface. (Harris, 1979; Berkeley & Rankey, 2012). It is hypothesized that the antecedent topography of the southern lineament assisted the stabilization of the island by providing a sediment baffle to sediment being transported westward (Fig. 12D). The eastern side of the island is wave-dominated, with fewer tidal channels and longer sections of coastline; the western side of the island exhibits more tidal dominance. Multiple lines of evidence, including radiocarbon data (Figs 2 and 3), aerial imagery (Fig. 11) and sedimentological relationships document the progradation of Little Ambergris Cay along both its southern and northern coasts to its form today (Fig. 12E).

Progradation along Holocene coasts is associated with a number of processes (Scheffers *et al.*, 2012; Tamura, 2012); it can be related to the delivery of sediment by longshore currents, waves and wind (Tamura, 2012); storms (Nott *et al.*, 2009; Scheffers *et al.*, 2012; Dougherty, 2014; Masselink & Van Heteren, 2014); possibly changes in sea level (Scheffers *et al.*, 2012; Tamura, 2012; Rivers *et al.*, 2020) and sedimentation supply (Tamura *et al.*, 2012) and rate. The seaward-dipping, shingling sediment packages on the south-western coast of the island (Fig. 5) record progradation of the beach face and, in some locations, aeolian dunes prograde over foreshore sediments and reach the waterline. These observations suggest that the progradation of the island was caused by fair-weather wave delivery of sediment to the shoreface, driven by easterly trade winds along the Ambergris shoal system.

Tropical cyclones and storms are implicated in the formation of beach ridges in other locations (Nott *et al.*, 2009; Dougherty, 2014; Masselink & Van Heteren, 2014). Modelling and observational study of the Great Bahama Bank suggests that hurricanes are not required to

explain the facies pattern of that nearby shallow-water carbonate platform (Lopez-Gamundi *et al.*, 2022). Detailed observations of the island before and after a direct hit by Hurricane Irma in 2017 (Jamison-Todd *et al.*, 2020; Lingappa *et al.*, 2022; Stein *et al.*, 2023) and observations of dune scarps after Hurricane Ike (Dravis & Wanless, 2017) suggest that storms are important erosive events on the island and contribute sediment to the island interior. Hurricane Irma likely submerged most of the island (Jamison-Todd *et al.*, 2020) and left deposits, now subaerially exposed, on the island. However, no new subaerial ridge on the island strandplain was observed following hurricanes Irma or Fiona; similar to the conclusions of a study from South Joulter's Cay (Harris & Laya, 2022), these observations suggest that although storms reshape the island and contribute to westward sediment transport, single storm events are unlikely to play a major role in the accretion of the island.

A sediment core collected from the island interior, VC03, includes three dated gastropod shells (Present *et al.*, 2021; Stein *et al.*, 2023) which may yield additional insight into the birth of Little Ambergris Cay (Table 2). The upper two shell ages reported from VC03, 402 to 926 cal yr BP and 574 to 1140 cal yr BP, record deposition synchronous with or post-dating initial intertidal deposition at the rim of the island. The units from which they derive would then reflect deposition in the interior of a rimmed island. The oldest shell reported from VC03 dates to 1944 to 2667 cal yr BP. There is no radiocarbon evidence for foreshore deposition on the lithified rim of Little Ambergris Cay during this interval, and it is possible that this depth in the core records deposition prior to development of the subaerially exposed island rim. The age of this shell is broadly concurrent with older dates from the Hanna Bay Member (described in The Bahamas) and could be interpreted as evidence for roughly modern sea level near Little Ambergris Cay by this time.

CONCLUSION

This study documents the recent and rapid growth of Little Ambergris Cay. Radiocarbon and sedimentological observations document that early synsedimentary lithification occurs rapidly on Little Ambergris Cay, and that such stabilization may be an important element of

island growth. Evidence that a precursor mid-Holocene aeolian dune system, now eroded, may have served as an important structural antecedent for the modern island was found. This precursor dune system is connected with the North Point Member, previously described from San Salvador. Other radiocarbon evidence suggests that the island began growing during the late Holocene Epoch. The ultimate accuracy of reported radiocarbon ages from the Ambergris system, and the Turks and Caicos platforms more broadly, requires establishing local marine reservoir corrections and evaluating the equilibrium of shallow, wind-swept waters with the atmosphere. Such considerations can shift the ages of samples by centuries, with important implications for archaeological, sea level and palaeoclimatic studies of the area. However, they do not impact the broader conclusions that exposed lithified sediments on the island are Holocene in age, or that recent, dynamic, change in Little Ambergris Cay's Holocene shoreline has occurred. It is concluded that Little Ambergris Cay's progradation and growth is primarily due to high sediment supply, low accommodation and sediment transport driven by easterly trade winds. The dynamism of this island should be considered in studies of the recent past – not only by Earth scientists seeking to reconstruct and interpret ancient shorelines, but also by archaeologists and biologists interested in reconstructing recent human and organismal dispersal across islands, as well as modern communities planning for the near future.

ACKNOWLEDGEMENTS

This work was supported by the 2016 and 2017 field seasons of the Agouon Foundation Advanced Geobiology School: thanks to participants Hannah Grotzinger, Usha Lingappa, Kyle Metcalfe, Daven Quinn, Leigh Anne Riedman, Sophia Roosth, Elizabeth Sibert, Cecilia Sanders, Freya Morris, Julien Alleon and Max Tarika for their assistance in the field. Credit for field photographs and photomicrographs is as follows: Emily Orzechowski (5A, 5B, 5C, 9D), Andrew H. Knoll (5D), Marjorie Cantine (5E, 5F, 5G, 5H, 6E, 6F, 7A, 7B, 7C, 8A, 8B, 8C, 8D, 9A, 9B, 9C), Justin V. Strauss (6A, 6B, 6C, 6D). Thanks to James Seymour for his capable piloting and knowledge of local history, and to Paul Mahoney and Shaun Austin for their help with field logistics. Thanks to the Tarika family for their hospitality. We

thank the Department of Coastal and Ecological Resources of the Turks and Caicos Islands and the Turks and Caicos National Trust for access to do research on Little Ambergris Cay under permits 16-06-02-10, 17-06-02-12, 18-02-04-05, 19-06-01-20 and 2022-05-11-25. NOSAMS is supported by the National Science Foundation (NSF) Cooperative Agreement OCE-1239667. Initial work for two seasons of study was supported by the Agouon Foundation Advanced Geobiology course. Subsequent work was supported by National Science Foundation grants OCE-2307830 to Trower, Cantine and Gomes and OCE-2032129 to Trower and Gomes; Agouon Institute Grant SGIA-277.19.1UCB to Trower and SGIA-277.19.1JHU to Gomes; NASA Grant 80NSSC18K0278 to Trower and Gomes. We thank C. Kerans, J.C. Laya and two anonymous reviewers for their reviews, and R. Sarg for his editorial handling.

DATA AVAILABILITY STATEMENT

All data is available within [Supporting Information](#).

REFERENCES

- Beaupré, S.R., Roberts, M.L., Burton, J.R. and Summons, R.E. (2015) Rapid, high-resolution ^{14}C chronology of ooids. *Geochim. Cosmochim. Acta*, **159**, 126–138.
- Berkeley, A. and Rankey, E.C. (2012) Progradational Holocene carbonate tidal flats of Crooked Island, southeast Bahamas: an alternative to the humid channelled belt model. *Sedimentology*, **59**, 1902–1925.
- Beverly, R.K., Beaumont, W., Taus, D., Ormsby, K.M., von Reden, K.F., Santos, G.M. and Southon, J.R. (2010) The Keck Carbon Cycle AMS Laboratory, University of California, Irvine: status report. *Radiocarbon*, **52**, 301–309.
- DiNapoli, R.J., Fitzpatrick, S.M., Napolitano, M.F., Rick, T.C., Stone, J.H. and Jew, N.P. (2021) Marine reservoir corrections for the Caribbean demonstrate high intra- and inter-island variability in local reservoir offsets. *Quat. Geochronol.*, **61**, 101126.
- Dougherty, A.J. (2014) Extracting a record of Holocene storm erosion and deposition preserved in the morphostratigraphy of a prograded coastal barrier. *Cont. Shelf Res.*, **86**, 116–131.
- Dravis, J.J. and Wanless, H.R. (2008) Caicos platform models of quaternary carbonate deposition controlled by stronger easterly trade winds—applications to petroleum exploration. In: *Developing Models and Analogs for Isolated Carbonate Platforms—Holocene and Pleistocene Carbonates of Caicos Platform, British West Indies*. SEPM Society for Sedimentary Geology, Tulsa, OK.
- Dravis, J.J. and Wanless, H.R. (2017) Impact of strong easterly trade winds on carbonate petroleum exploration—relationships developed from Caicos Platform, southeastern Bahamas. *Mar. Pet. Geol.*, **85**, 272–300.

- Duguid, S.M.A., Kyser, T.K., James, N.P. and Rankey, E.C. (2010) Microbes and Ooids. *J. Sed. Res.*, **80**, 236–251.
- Emery, K.O. (1955) Transportation of Rocks by Driftwood. *J. Sed. Res.*, **25**, 51–57. <https://doi.org/10.1306/D42697FB-2B26-11D7-8648000102C1865D>.
- Emery, K.O. and Tschudy, R.H. (1941) Transportation of rock by kelp. *Geol. Soc. Am. Bull.*, **52**, 855–862.
- Falkenroth, M., Green, A.N., Cooper, J.A.G., Menzel, M.D. and Hoffmann, G. (2022) Breaking up and making up—reworking of Holocene calcarenite platform into rapidly-forming beachrock breccias on a high energy coastline (St. Lucia, South Africa). *Sedimentology*, **69**, 1339–1364.
- Flessa, K.W., Cutler, A.H. and Meldahl, K.H. (1993) Time and taphonomy: quantitative estimates of time-averaging and stratigraphic disorder in a shallow marine habitat. *Paleobiology*, **19**, 266–286.
- Garden, C.J. and Smith, A.M. (2015) Voyages of seaweeds: the role of macroalgae in sediment transport. *Sediment. Geol.*, **318**, 1–9.
- Gerber, G.P., Colosimo, G.G. and Tandora, D. (2020) *Cyclura carinata*. The IUCN Red List of Threatened Species 2020.
- Godefroid, F. (2011) Géologie de Mayaguana, SE de l'archipel des Bahamas. PhD thesis, Université de Genève.
- Godwin, H. (1962) Half-life of Radiocarbon. *Nature*, **195**, 984.
- Gomes, M.L., Riedman, L.A., O'Reilly, S., Lingappa, U., Metcalfe, K., Fike, D.A., Grotzinger, J.P., Fischer, W.W. and Knoll, A.H. (2020) Taphonomy of biosignatures in microbial mats on Little Ambergris Cay, Turks and Caicos Islands. *Front. Earth Sci.*, **8**, 576712. <https://doi.org/10.3389/feart.2020.576712>.
- Halley, R.B. and Harris, P.M. (1979) Fresh-water cementation of a 1000-year old oolite. *J. Sediment. Petrol.*, **49**, 969–988.
- Hardman, C.J., Williams, S., Manco, B.N. and Hamilton, M.A. (2012) Predicting the potential threat of *Casuarina equisetifolia* to three endemic plant species on The Turks and Caicos Islands. *Oryx*, **46**, 204–212.
- Harris, M. (1979) Facies anatomy and diagenesis of a Bahamian Ooid Shoal. In: *Sedimenta VII*. The Comparative Sedimentology Laboratory, Division of Marine Geology and Geophysics, University of Miami, Rosenstiel School of Marine & Atmospheric Science, Miami, FL.
- Harris, P. and Laya, J.C. (2022) Evolution of a Modern Ooid Sand Island (South Joulter Cay, Great Bahama Bank) and implications for subsurface studies. In: *2022 International Meeting for Applied Geoscience & Energy*. American Association of Petroleum Geologists, Tulsa, OK.
- Haslett, J. and Parnell, A. (2008) A simple monotone process with application to radiocarbon-dated depth chronologies. *J. R. Stat. Soc. Ser. C. Appl. Stat.*, **57**, 399–418.
- Hearty, P.J. and Kindler, P. (1993) New perspectives on Bahamian Geology: San Salvador Island, Bahamas. *Source J. Coast. Res.*, **9**, 74.
- Heaton, T.J., Köhler, P., Butzin, M., Bard, E., Reimer, R.W., Austin, W.E.N., Bronk Ramsey, C., Grootes, P.M., Hughen, K.A., Kromer, B., Reimer, P.J., Adkins, J., Burke, A., Cook, M.S., Olsen, J. and Skinner, L.C. (2020) Marine20—the marine radiocarbon age calibration curve (0–55,000 cal BP). *Radiocarbon*, **62**, 779–820.
- Horton, B.P., Khan, N.S., Cahill, N., Lee, J.S.H., Shaw, T.A., Garner, A.J., Kemp, A.C., Engelhart, S.E. and Rahmstorf, S. (2020) Estimating global mean sea-level rise and its uncertainties by 2100 and 2300 from an expert survey. *NPJ Clim. Atmos. Sci.*, **3**, 18. <https://doi.org/10.1038/s41612-020-0121-5>.
- Jamison-Todd, S., Stein, N., Overeem, I., Khalid, A. and Trower, E.J. (2020) Hurricane deposits on carbonate platforms: a case study of Hurricane Irma Deposits on Little Ambergris Cay, Turks and Caicos Islands. *J. Geophys. Res. Earth Surf.*, **124**, e2020JF005597. <https://doi.org/10.1029/2020JF005597>.
- Kerans, C., Zahm, C., Bachtel, S.L., Hearty, P. and Cheng, H. (2019) Anatomy of a late quaternary carbonate island: constraints on timing and magnitude of sea-level fluctuations, West Caicos, Turks and Caicos Islands, BWI. *Quat. Sci. Rev.*, **205**, 193–223.
- Khan, N.S., Ashe, E., Horton, B.P., Dutton, A., Kopp, R.E., Brocard, G., Engelhart, S.E., Hill, D.F., Peltier, W.R., Vane, C.H. and Scatena, F.N. (2017) Drivers of Holocene sea-level change in the Caribbean. *Quat. Sci. Rev.*, **155**, 13–36.
- Kindler, P. and Hearty, P.J. (1996) Carbonate petrography as an indicator of climate and sea-level changes: new data from Bahamian Quaternary units. *Sedimentology*, **43**, 381–399.
- Kirezci, E., Young, I.R., Ranasinghe, R., Muis, S., Nicholls, R.J., Lincke, D. and Hinkel, J. (2020) Projections of global-scale extreme sea levels and resulting episodic coastal flooding over the 21st Century. *Sci. Rep.*, **10**, 11629.
- Lindsey, B. (2021) Historic Glass Bottle Identification & Information. <https://sha.org/bottle/index.htm>. Accessed 24 Apr 2023.
- Lingappa, U.F., Stein, N.T., Metcalfe, K.S., Present, T.M., Orphan, V.J., Grotzinger, J.P., Knoll, A.H., Trower, E.J., Gomes, M.L. and Fischer, W.W. (2022) Early impacts of climate change on a coastal marine microbial mat ecosystem. *Sci. Adv.*, **8**, eabm7826.
- Lloyd, R.M., Perkins, R.D. and Kerr, S.D. (1987) Beach and shoreface ooid deposition on shallow interior banks, Turks and Caicos Islands, British West Indies. *J. Sed. Res.*, **57**, 976–982. <https://doi.org/10.1306/212F8CBF-2B24-11D7-8648000102C1865D>.
- Lokier, S. and Steuber, T. (2008) Quantification of carbonate-ramp sedimentation and progradation rates for the late Holocene Abu Dhabi shoreline. *J. Sed. Res.*, **78**, 423–431.
- Lopez-Gamundi, C., Dobbelaere, T., Hanert, E., Harris, P.M., Eberli, G. and Purkis, S.J. (2022) Simulating sedimentation on the Great Bahama Bank—sources, sinks and storms. *Sedimentology*, **69**, 2693–2714.
- Malooof, A.C. and Grotzinger, J.P. (2012) The Holocene shallowing-upward parasequence of north-west Andros Island, Bahamas. *Sedimentology*, **59**, 1375–1407.
- Masselink, G. and van Heteren, S. (2014) Response of wave-dominated and mixed-energy barriers to storms. *Mar. Geol.*, **352**, 321–347.
- McCutcheon, J., Nothdurft, L.D., Webb, G.E., Paterson, D. and Southam, G. (2016) Beachrock formation via microbial dissolution and re-precipitation of carbonate minerals. *Mar. Geol.*, **382**, 122–135.
- McCutcheon, J., Nothdurft, L.D., Webb, G.E., Shuster, J., Nothdurft, L., Paterson, D. and Southam, G. (2017) Building biogenic beachrock: Visualizing microbially-mediated carbonate cement precipitation using XFM and a strontium tracer. *Chem. Geol.*, **465**, 21–34.
- Milne, G.A. and Peros, M. (2013) Data-model comparison of Holocene sea-level change in the circum-Caribbean region. *Glob. Planet. Chang.*, **107**, 119–131.

- Milne, G., Long, A. and Bassett, S. (2005) Modelling Holocene relative sea-level observations from the Caribbean and South America. *Quat. Sci. Rev.*, **24**, 1183–1202.
- Myroie, J.E. and Carew, J.L. (1995) Geology and karst geomorphology of San Salvador Island, Bahamas. *Carbonates Evaporites*, **10**, 193–206.
- Myroie, J.E., Carew, J.L., Curran, H.A., Martin, J.B., Rothfus, T.A., Myroie, J.E., Carew, J.L., Curran, H., Allen, Martin, J.B., Rothfus, T.A., Sealey, N.E. and Siewers, F.D. (2008) Geology of Rum Cay, Bahamas: a Field Trip Guide Geology of Rum Cay, Bahamas: A Field Trip Guide.
- Nicholls, R.J. (2011) Planning for the impacts of Sea Level Rise. *Oceanography*, **24**, 144–157.
- Nott, J., Smithers, S., Walsh, K. and Rhodes, E. (2009) Sand beach ridges record 6000 year history of extreme tropical cyclone activity in northeastern Australia. *Quat. Sci. Rev.*, **28**, 1511–1520.
- Orzechowski, E., Strauss, J.V., Knoll, A.H., Fischer, W.W., Cantine, M.D., Metcalfe, K.S., Quinn, D.P., Stein, N.T., Gomes, M.L., Grotzinger, J.P., Lingappa, U.F., O'Reilly, S.S., Riedman, L.A. and Trower, E.J. (2016) Age and construction of Little Ambergris Cay Bedrock Rim, Southeastern Caicos Platform, British West Indies. In: AGU Fall Meeting Abstracts.
- Pearson, A., McNichol, A.P., Schneider, R.J., Von Reden, K.F. and Zheng, Y. (1997) Microscale AMS ^{14}C measurement at NOSAMS. *Radiocarbon*, **40**, 61–75.
- Peter, G.R.F.D. and Gould, S.J. (1984) Geology of New Providence Island, Bahamas. *Geol. Soc. Am. Bull.*, **95**, 209–220.
- Planet Team. (2022) Planet Application Program Interface: Space for Life on Earth. <https://api.planet.com>. Accessed 23 Apr 2023.
- Present, T.M., Gomes, M.L., Trower, E.J., Stein, N.T., Lingappa, U.F., Naviaux, J., Thorpe, M.T., Cantine, M.D., Fischer, W.W., Knoll, A.H. and Grotzinger, J.P. (2021) Non-lithifying microbial ecosystem dissolves peritidal lime sand. *Nat. Commun.*, **12**, 1–8.
- Rankey, E.C., Reeder, S.L. and Correa, T.B.S. (2008) Geomorphology and Sedimentology of Ambergris Ooid Shoal, Caicos Platform. In: *Developing models and analogs for isolated carbonate platforms—holocene and pleistocene carbonates of Caicos Platform, British West Indies*. SEPM Society for Sedimentary Geology, Tulsa, OK.
- Raven, M.R., Fike, D.A., Gomes, M.L. and Webb, S.M. (2019) Chemical and isotopic evidence for organic matter sulfuration in redox gradients around mangrove roots. *Front. Earth Sci.*, **7**, 98. <https://doi.org/10.3389/feart.2019.00098>.
- Reimer, P.J. and Reimer, R.W. (2001) A marine reservoir correction database and on-line interface. *Radiocarbon*, **43**, 461–463.
- Reimer, P.J., Austin, W.E.N., Bard, E., Bayliss, A., Blackwell, P.G., Bronk Ramsey, C., Butzin, M., Cheng, H., Edwards, R.L., Friedrich, M., Grootes, P.M., Guilderson, T.P., Hajdas, I., Heaton, T.J., Hogg, A.G., Hughen, K.A., Kromer, B., Manning, S.W., Muscheler, R., Palmer, J.G., Pearson, C., van der Plicht, J., Reimer, R.W., Richards, D.A., Scott, E.M., Southon, J.R., Turney, C.S.M., Wacker, L., Adolphi, F., Büntgen, U., Capano, M., Fahrni, S.M., Fogtmann-Schulz, A., Friedrich, R., Köhler, P., Kudsk, S., Miyake, F., Olsen, J., Reinig, F., Sakamoto, M., Sookdeo, A. and Talamo, S. (2020) The IntCal20 Northern Hemisphere radiocarbon age calibration curve (0–55 cal kBP). *Radiocarbon*, **62**, 725–757.
- Reynolds, R.G., Gerber, G.P., Burgess, J.P., Waters, G.H. and Manco, B.N. (2020) Characterization of color pattern dimorphism in Turks and Caicos Boas, *Chilabothrus chrysogaster chrysogaster*, on Big Ambergris Cay, Turks and Caicos Islands. *J. Herpetol.*, **54**, 337–346. <https://doi.org/10.1670/18-051>.
- Rivers, J.M., Dalrymple, R.W., Yousif, R., Al-Shaikh, I., Butler, J.D., Warren, C., Skeat, S.L. and Abdel Bari, E.M.M. (2020) Mixed siliciclastic-carbonate-evaporite sedimentation in an Arid Eolian Landscape: the Khor Al Adaid Tide-Dominated Coastal Embayment, Qatar. *Sediment. Geol.*, **408**, 105730. <https://doi.org/10.1016/j.sedgeo.2020.105730>.
- Scheffers, A., Engel, M., Scheffers, S., Squire, P. and Kelletat, D. (2012) Beach ridge systems - archives for Holocene coastal events? *Prog. Phys. Geogr.*, **36**, 5–37.
- Stein, N., Grotzinger, J.P., Hayden, A., Quinn, D.P., Trower, L., Lingappa, U., Present, T.M., Gomes, M., Orzechowski, E.A. and Fischer, W.W. (2017) Impact of Hurricane Irma on Little Ambergris Cay, Turks and Caicos. American Geophysical Union Fall Meeting Abstracts.
- Stein, N.T., Grotzinger, J.P., Quinn, D.P., Lingappa, U.F., Present, T.M., Trower, E.J., Gomes, M.L., Orzechowski, E., Cantine, M., Metcalfe, K.S., Fischer, W.W., Ehlmann, B.L., Strauss, J.V. and Knoll, A.H. (2023) Geomorphic and Environmental Controls on Microbial Mat Fabrics on Little Ambergris Cay, Turks and Caicos Islands. *Sedimentology*, **70**, 1915–1944. <https://doi.org/10.1111/sed.13100>.
- Strasser, A. and Davaud, E. (1986) Formation of Holocene limestone sequences by progradation, cementation, and erosion: two examples from The Bahamas. *J. Sediment. Petrol.*, **56**, 422–428.
- Strauss, B.H., Orton, P.M., Bittermann, K., Buchanan, M.K., Gilford, D.M., Kopp, R.E., Kulp, S., Massey, C., de Moel, H. and Vinogradov, S. (2021) Economic damages from Hurricane Sandy attributable to sea level rise caused by anthropogenic climate change. *Nat. Commun.*, **12**, 2720.
- Stuiver, M. and Polach, H.A. (1977) Reporting of ^{14}C data. *Radiocarbon*, **19**, 355–363.
- Tamura, T. (2012) Beach ridges and prograded beach deposits as palaeoenvironment records. *Earth Sci. Rev.*, **114**, 279–297.
- Tamura, T., Saito, Y., Lap Nguyen, V., Oanh Ta, T.K., Bateman, M.D., Matsumoto, D. and Yamashita, S. (2012) Origin and evolution of interdistributary delta plains; insights from Mekong River Delta. *Geology*, **40**, 303–306.
- Trembath-Reichert, E., Ward, L.M., Slotznick, S.P., Bachtel, S.L., Kerans, C., Grotzinger, J.P. and Fischer, W.W. (2016) Gene sequencing-based analysis of microbial-mat morphotypes, Caicos Platform, British West Indies. *J. Sed. Res.*, **86**, 629–636.
- Trower, E.J., Cantine, M.D., Gomes, M.L., Grotzinger, J.P., Knoll, A.H., Lamb, M.P., Lingappa, U., O'Reilly, S.S., Present, T.M., Stein, N., Strauss, J.V. and Fischer, W.W. (2018) Active ooid growth driven by sediment transport in a high-energy shoal, Little Ambergris Cay, Turks and Caicos Islands. *J. Sed. Res.*, **88**, 1132–1151.
- Wanless, H.R., Harold, R. and Dravis, J.J. (1989) *Carbonate Environments and Sequences of Caicos Platform: Caicos, British West Indies to Miami, Florida, July 20–26, 1989 (Field Trip Guidebook T374)*. American Geophysical Union, Washington, D.C.

- Ward, L.M., Lingappa, U.F., Grotzinger, J.P. and Fischer, W.W.** (2020) Microbial mats in The Turks and Caicos Islands reveal diversity and evolution of phototrophy in the Chloroflexota order *Aggregatilineales*. *Environ. Microbiomes*, **15**, 9.
- White, B. and Curran, H.A.** (1988) Mesoscale physical sedimentary structures and trace fossils in Holocene carbonate eolianites from San Salvador Island, Bahamas. *Sediment. Geol.*, **55**, 163–184.
- Wiles, E., Green, A.N. and Cooper, J.A.G.** (2018) Rapid beachrock cementation on a South African beach: linking morphodynamics and cement style. *Sediment. Geol.*, **378**, 13–18.
- Wu, M., Harris, P., Eberli, G. and Purkis, S.J.** (2021) Sea-level, storms, and sedimentation – controls on the architecture of the Andros tidal flats (Great Bahama Bank). *Sediment. Geol.*, **420**, 105932.

Manuscript received 11 July 2023; revision accepted 15 April 2024

Supporting Information

Additional information may be found in the online version of this article:

Figure S1. Calibrated radiocarbon ages with probability distributions for all samples.

Figure S2. Map showing the distribution of lithified sediments and cover on Little Ambergris Cay.

Table S1. Names and coordinates of all stratigraphic sections on Little Ambergris Cay explored in this study.

Table S2. All radiocarbon data and results of sensitivity tests explored in Appendix S2.

Table S3. Results from analysis of seawater samples taken near Little Ambergris Cay, discussed in Supporting Information.

Appendix S1. Text describing sensitivity tests shown in Table S2.

Appendix S2. Supplementary stratigraphic columns and associated location map.